

PHYSICAL REVIEW D

PARTICLES AND FIELDS

THIRD SERIES, VOLUME 29, NUMBER 11

1 JUNE 1984

Measurement of $\Delta\sigma_L$ and $C_{LL}=(L,L;0,0)$ in proton-proton scattering between 300 and 800 MeV

I. P. Auer,* W. R. Ditzler, D. Hill, K. Imai,[†] H. Spinka, R. Stanek, K. Toshioka,[‡]
D. Underwood, R. Wagner, and A. Yokosawa
Argonne National Laboratory, Argonne, Illinois 60439

E. W. Hoffman and J. J. Jarmer
Los Alamos National Laboratory, Los Alamos, New Mexico 87545

G. R. Bureson, W. B. Cottingham, S. J. Greene,[§] and S. Stuart**
Department of Physics, New Mexico State University, Las Cruces, New Mexico 88003
(Received 27 December 1983)

Measurements are reported of the difference $\Delta\sigma_L$ between proton-proton total cross sections for parallel and antiparallel spin states and of the parameter C_{LL} for proton-proton elastic scattering near 90° , for thirteen energies between 300 and 800 MeV. The $\Delta\sigma_L$ results agree well with previous ANL ZGS and SIN data, but disagree with recent results from TRIUMF. Attempts to understand the cause of the discrepancy have been unsuccessful, but possible sources are discussed. The $\Delta\sigma_L$ and C_{LL} results have been used with other experimental data to extract quantities which depend only on spin-singlet, coupled spin-triplet, and spin-triplet partial waves. Structure is found in these quantities, which appears to be associated with the resonantlike 1D_2 and 3F_3 partial waves. Additional similar structure is also found, which may be due either to the 3P_0 partial wave or the ($^3P_2, ^3F_2$) partial-wave pair.

I. INTRODUCTION

Since the discovery of structure in proton-proton total cross sections in pure spin states several years ago, which led to suggestions of the existence of pp resonances,¹ there has been great interest in the general subject of dibaryon resonances. Before this, it was generally believed that such resonances do not exist, partly because of the absence of any indication of resonance structure in the spin-averaged pp and pn total cross sections and partly because of the lack of any apparent need for dibaryon resonances in the symmetry schemes for hadrons that had been current. From a dynamical point of view, however, there is no reason for such objects not to exist, and in particular, one (the deuteron) does exist as a bound state. There have been models discussed in the literature for others, including hadron-hadron states² such as $N-\Delta$ and $\Delta-\Delta$, as well as six-quark objects.³ Furthermore, if $S=0$ dibaryons exist, it is reasonable to expect $S\neq 0$ dibaryons to exist also (and vice versa); the evidence for strange dibaryons has also been summarized recently.⁴ As of now, however, the understanding of dibaryons has not reached the stage where the patterns associated with them (if they exist) can be perceived.

The subject has been, and still is, a somewhat contro-

versial one, with much evidence both for and against such resonances having been presented; fairly detailed summaries of the current status of dibaryon resonances have been given.⁵ Recently, massive data on spin-spin correlation parameters from 1.18 to 2.47 GeV/c have become available;⁶ they give a decisive clarification of the structure in the pp system as supporting the existence of diproton resonances and disagree with predictions of theoretical models⁷ which might not describe short-range nucleon-nucleon interactions properly. The principal experimental evidence that has been interpreted as favoring pp resonances includes measurements of the differences between total cross sections $\Delta\sigma_L$ (Ref. 1) and $\Delta\sigma_T$ (Ref. 8) for pure longitudinal and transverse spin states, measurements of various parameters in elastic scattering, such as polarization and spin-spin correlation tensors, and various results from inelastic channels.⁹ These data have been the subject of much phenomenological and theoretical study, which has produced some apparently contradictory results. The phase-shift analyses of Hoshizaki¹⁰ and Bhandari, Arndt, Roper, and VerWest¹¹ have indicated resonantlike behavior in the 1D_2 and 3F_3 partial waves; in the latter, model fits were made which revealed poles in these waves near the $N-\Delta$ threshold. Amplitude analyses of Grein and Kroll^{12,13} based on dispersion relations indi-

cated structures in the 3F_3 and 1G_4 partial waves which might be caused by dibaryon resonances, and an energy dependence in the 1D_2 partial wave which could be interpreted most easily as a threshold effect. Recent phase-shift results from Saclay,¹⁴ however, indicate a resonance-like behavior in the 1D_2 , but not the 3F_3 , partial wave.

A criticism of these results and these interpretations was noted by Bugg,¹⁵ however, who claimed that the $\Delta\sigma_L$ data below 800 MeV disagree with the (BASQUE) phase-shift analysis of Bugg *et al.*,¹⁶ as well as with conventional models of the inelastic channels. Other criticisms of the interpretations of the behavior of the phase shifts as being due to resonances have been given by Hollas¹⁷ and by Kloet and Silbar,¹⁸ who claimed that mechanisms other than resonances could be responsible. Niskanen¹⁹ has shown that these apparent resonances could all simply be reflections of the opening of real $N\Delta$ channels.

Because the conjectured resonances are likely to be highly inelastic, investigations of inelastic channels have been made also. In one of these, Bolger *et al.*²⁰ measured the asymmetry in π^+d elastic scattering with a vector-polarized deuteron target and found a rapid variation consistent in some cases with the presence of one or more dibaryon resonances. It has been shown by Arvieux,²¹ however, that some of the observed behavior could also be produced by small variations in nonresonant amplitudes. Measurements of the tensor polarization in π^+d scattering, however, indicate some kind of unconventional dynamics, which may be related to dibaryons, but unfortunately disagree with each other.²² Experimental studies of photodisintegration of the deuteron have found indications both for^{2,23} and against²⁴ dibaryons. Other examples of conflicting evidence similar to these also exist.⁵

Considerations such as these were among the principal motivations that led us to undertake the experiment reported here, a remeasurement of $\Delta\sigma_L$ at energies between 300 and 800 MeV, together with a measurement of the spin-correlation parameter $C_{LL} = (L, L; 0, 0)$ near 90° (c.m.), carried out at the Clinton P. Anderson Meson Physics Facility (LAMPF), at Los Alamos. Another motivation was to search for additional narrow structure, the existence of which could not be ruled out by existing data.²⁵ For this reason, finer energy steps were taken than had been used before in this work. The C_{LL} data were measured at the same time as $\Delta\sigma_L$, as had been done before.²⁶ The earlier results on C_{LL} had been fairly important in the modification of existing phase shifts, particularly those of Bhandari, Arndt, Roper, and VerWest.¹¹ Some results on both of these measurements have been reported in short articles.^{27,28} The $\Delta\sigma_L$ results agree with the previous data from Argonne, as well as with preliminary data from SIN,²⁹ but disagree significantly with new data from TRIUMF.³⁰ The C_{LL} data agree with previous results and indicate evidence for another possible resonance in one of the 3P partial waves, as discussed below.

The disagreement among the various sets of $\Delta\sigma_L$ data is well outside of estimated experimental error and is a cause for concern. Extensive discussions with the TRIUMF group have led to small changes in numerical values of both sets of data, but have not been successful in resolving the differences between them. Similar differ-

ences have also been found between the TRIUMF $\Delta\sigma_T$ data and new measurements of $\Delta\sigma_T$ made by us at LAMPF (Ref. 31) subsequent to the work reported here.

In phase-shift analysis, the values of $\Delta\sigma_L$ used have important effects in the inelasticities required for certain partial waves.³⁰ It has been possible to find solutions which fit either data set. The solutions of Bhandari, Arndt, Roper, and VerWest incorporate the new data reported here but cannot accommodate the TRIUMF data.³² The Saclay solution¹⁴ also passes through the LAMPF-Argonne-SIN data. The BASQUE solution incorporates all data, but with a large normalization adjustment, and passes through the TRIUMF data.³⁰ The amplitude analysis of Grein and Kroll,¹³ however, found discrepancies in the BASQUE phase shifts which caused them to be unable to conclude that they are in agreement with forward dispersion relations. It was later noted by Axen *et al.*,³⁰ though, that satisfactory agreement can be obtained by a small change in certain contributions to that solution. They also point out that phase-shift solutions which pass through the LAMPF-Argonne-SIN data required surprisingly large inelasticities in certain partial waves, a result not supported by data from the $pp \rightarrow \pi d$ channel alone. More discussion of these discrepancies is given below.

Details of the experimental setup used are discussed below in Sec. II. The analysis of the data and comparisons to other data are discussed in Sec. III. Interpretations of the results are discussed in Sec. IV, and a summary is given in Sec. V. Because of the importance of the discrepancies between these results and those of the TRIUMF group, we have provided a fair amount of detail of the methods and procedures used in carrying out the experiment and in analyzing the data.

II. EXPERIMENTAL SETUP

A. Beam

1. The LAMPF polarized-beam facility

The LAMPF Lamb-shift polarized-ion source³³ produces an H^- beam with polarization as high as 0.9 at about 10 nA of current. This beam is accelerated through the linear accelerator simultaneously with the more intense H^+ (proton) beam on alternate half cycles of the 201-MHz rf voltage to energies as high as 800 MeV. The duty factor for this mode is typically 9%. For energies less than 800 MeV, the proton source is inhibited and the acceleration of the H^- beam ceases at the rf module corresponding to the desired energy. The sum of the proton- and H^- -beam duty factors may be 9%, with any sharing allowed that is consistent with the 120-Hz repetition rate of the acceleration cycle.

The accelerated polarized H^- beam is easily separated into an H^- and a proton beam by using a thin foil to strip part of the beam and a dipole magnet to spatially separate the two species. This operation is normally performed twice at two successive locations to produce three simultaneous polarized beams, two proton beams (lines B and C) and one H^- external proton beam (EPB). The beam

line used for this measurement has its source in the hole of the second set of stripper foils and begins as H^- . This source can vary in transverse dimensions from 0 to 0.5 cm in the vertical and horizontal. The beam divergence at the source stripper hole is typically 0.15 mr. For low beam currents, as used in this measurement, the stripper aperture was usually less than 1 mm in each dimension. With no multiple scattering, the beam optics should produce a spot about 1 mm in diameter at the position of the polarized target.

For this experiment, the beam was usually accelerated with the polarization in an N -type³⁴ (vertical) orientation. Midway through the EPB line a spin precessor³⁵ reoriented the spin to the desired direction, which was normally L -type (longitudinal). This precessor, which consisted of a solenoid, three dipoles and a 12- μm mylar stripper, used precession of H^- , subsequent conversion to H^+ , and additional precession to produce an undeflected beam of arbitrarily selected spin orientation. The beam impinging on the polarized target was always a clean, polarized proton beam, since a change in the sign of the charge was required midway through the spin precessor. The kinetic energies of the beam were found from the accelerator parameters, with corrections for energy loss to the center of the polarized target.

2. Beam-polarization measurements

The beam polarization was monitored by polarimeters^{36,37} available in two of the polarized beam lines (EPB and line B), which utilized pp elastic scattering from a CH_2 target. Elastic scatters were detected by a coincidence between both the scattered and recoil protons near 40° (c.m.), where the analyzing power has a broad maximum. The laboratory angles of the recoil scintillators were changed as required to accommodate the energy dependence of the kinematics. The analyzing power is high³⁸ throughout the energy region covered. Another polarimeter, constructed for this experiment, was located downstream of the polarized target. There, elastic pp scatters from a liquid-hydrogen (LH_2) target were used to obtain a polarization measurement which was independent of the carbon contribution from the CH_2 targets.

The usefulness of the polarization measurements in each polarimeter depended on the beam intensity and polarization orientation. The beam polarization for individual data runs was normally monitored by the line-B polarimeter, and the LH_2 polarimeter in EPB was used to extract an average beam polarization for the sum of all runs at each beam energy. Insufficient data rates in the hydrogen polarimeter prevented its use as a monitor for individual runs.

A typical scenario for each energy was to tune the optics and steering for the new energy, calibrate the beam-line polarimeters against the beam polarization as determined by the quench-ratio method (described below) with a high-intensity N -type beam, calibrate the LH_2 polarimeter against the quench ratio with an S -type beam (polarized horizontally, perpendicular to the beam direction) at the polarimeter, and set all beam intensities to the desired levels for data taking.

3. The LH_2 polarimeter

This polarimeter, which is described in detail elsewhere,^{39,40} was located downstream of the polarized target. The L -type beam passed through several scintillation counters and wire chambers, as well as through the polarized target, and was then bent in a horizontal plane by a bending magnet (named LILLY) so that the spin direction was precessed 90° to the S direction. The up-down asymmetry was then measured, to give the L -type polarization of the beam at the polarized target. The S -type component was determined by the EPB polarimeter (upstream of the experiment), and the N -type component with both polarimeters.

After LILLY, the beam passed through a 0.9-m-long steel collimator with a 6.4-cm-diameter hole. The collimator was surrounded by lead bricks and lead wool and served to eliminate particles that had interacted in the polarized target or other material in the beamline or beam particles that had suffered a large amount of multiple scattering. Following the collimator were scintillation counters (described below) and the liquid-hydrogen target for the LH_2 polarimeter.

The LH_2 target was located 2.4-m downstream of LILLY. The beam entered the vacuum surrounding the target through an 8.9-cm-diameter window of 0.13-mm-thick mylar. After traversing about 9 cm of vacuum, the beam entered the 17.8-cm-long-by-7.6-cm-diameter target flask containing the liquid hydrogen. The flask was constructed of 0.13-mm-thick mylar and surrounded by 10 layers of 6.4- μm aluminized mylar insulation. In addition to the target flask and insulation, the forward and recoil protons had to pass through the 1.6-mm-thick aluminum vacuum vessel on the way to the polarimeter counters. The vessel shape was a section of a right circular cone with half-angle 30° with its symmetry axis along the beamline. The tip of the cone was replaced by a section of a sphere, which was located roughly 1 cm beyond the hemispherical end of the target flask. Externally, the vacuum vessel resembled a rocket nose cone.

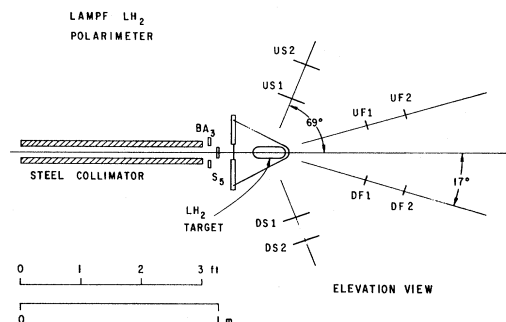


FIG. 1. Schematic diagram of the up-down portion of the liquid-hydrogen (LH_2) polarimeter. UF_1 and UF_2 were scintillation counters detecting a forward-going proton scattered up, and DS_1 and DS_2 were counters detecting in coincidence the proton scattered down; the angles were set for the kinematics of elastic scattering. DF_1 and DF_2 , together with US_1 and US_2 , detected the corresponding event with the forward-going proton scattered down. The counters corresponding to left-right scattering are not shown.

The LH₂ polarimeter geometry is shown in Fig. 1. In addition to the counters shown, there were sets of left and right counters similar to the up and down counters. There were also large scintillators placed farther from the target which covered an increased solid angle and which were primarily used to monitor the beam polarization in the *S*-type direction at the polarimeter. With the exception of these large scintillators, the counters downstream of the LH₂ target were mounted in a cylindrically shaped structure with the axis on the beamline. The structure was designed so that it could rotate about its axis for tests of instrumental asymmetries. The entire polarimeter, including the collimator, some triggering counters, the LH₂ target, the scintillators, and the cylindrical mounting structure were mounted on a cart that rolled on the floor and pivoted about a point beneath LILLY. Lines surveyed on the floor were used when adjusting the polarimeter angle relative to the beam direction upstream of LILLY. At each angle, the polarimeter elevation was adjusted with jacks to put its axis on the beam height.

4. Calibration of the polarimeters

The calibration of polarimeters at LAMPF has generally been performed using the quench-ratio technique.^{36,38,41,42} This method relies on the atomic physics of the ion source and the assumption of a lack of depolarization between the ion source and the polarimeter in the experimental area. Calculations and various tests indicate that the latter assumption is correct to better than 1% under normal conditions.^{36,43} The calibration is performed by measuring a ratio of intensities with the beam polarized and with the beam quenched at the ion source. In the latter condition, the polarized protons are removed and the unpolarized background protons are left in the beam.

For the hydrogen-polarimeter calibration, the beam polarization P_B was determined using the quench-ratio technique, and the asymmetry ϵ in the polarimeter was measured simultaneously. The polarimeter calibration constant A_p is defined as $A_p = \epsilon/P_B$. If the events detected were purely from *pp* elastic scattering, then, in principle, the value of A_p could be calculated from the *pp* polarization parameter (or analyzing power) as a function of angle, the polarimeter acceptance, and energy-loss and multiple-scattering effects. In practice, there were also contributions to the detected events from inelastic reactions and from quasielastic reactions on other nuclei in or near the polarimeter target.

There were two methods used to measure the LH₂-polarimeter calibration constant. At seven energies the quench-ratio technique was used directly. The beam was first tuned down the EPB line with a beam intensity roughly an order of magnitude higher than normal. It was then verified that the beam spin was purely *L*-type at the polarized target and purely *S*-type at the LH₂ target, using the EPB and LH₂ polarimeters. The beam-intensity ratio during polarized and quenched periods was monitored by the sum of the left and right counts in the LH₂ polarimeter.

The second method used to obtain the calibration con-

stant was less direct. First the EPB polarimeter was calibrated in the usual way with an *N*- or *S*-type beam using the quench-ratio technique. An *S*-type beam was used at the polarized target and the polarimeter was set to 0° with LILLY turned off. Thus, the beam spin was also *S*-type at the LH₂ target. Then the asymmetries for the EPB and LH₂ polarimeters were measured simultaneously, and the LH₂ calibration constant was determined from these data.

There is one feature of the setup which could bring the calibrations of the LH₂ polarimeter into question. The beam passed through a large quantity of material between the end of EPB and the center of the LH₂ target, which caused a considerable amount of multiple scattering. As a consequence, the beam spot was quite large at the collimator before the LH₂ target, so that only about 20% of the beam was transmitted. Therefore, the LH₂ target was nearly uniformly illuminated by the beam particles. The multiple scattering and beam energy loss could have led to some beam depolarization. Theoretically, this depolarization should have been quite small.⁴⁴ This was tested at 800 MeV with the polarized target in and out of the beam. The two measured calibration constants agreed, with an uncertainty of $\pm 2\%$, indicating that the effect was small. The polarimeter calibration found during the experimental runs agreed quite well with the measurements of McNaughton and Chamberlin³⁸ when corrections were made for the acceptance and background.^{39,40}

B. Polarized target

1. The target

The polarized proton target (PPT) was a continuously polarizing type utilizing microwave dynamic nuclear cooling.⁴⁵ The target material was 1,2-propanediol, doped with potassium dichromate and frozen in the form of ~ 2 -mm-diameter beads. The field of the target magnet was parallel to the beam momentum, producing a longitudinal polarization. The target, 5.5 cm in length and 2 cm in diameter, was cooled by a vertical continuous-flow ³He refrigerator with ⁴He precooling, producing temperatures of less than 0.5 K. The polarization was monitored with nuclear magnetic resonance (NMR) and was measured to be typically 80%, with a characteristic reversing time constant of about 7 min. The microwave source was a carcinotron operating with a frequency near 70 GHz. All critical target monitors and controls were located remotely from the experimental hall.

2. The target magnet

The magnet, known as HERA, consisted of a pair of Helmholtz coils which produced a 2.5-T field, homogeneous to within 0.8 mT throughout the target volume. The superconducting magnet and ³He refrigerator were originally constructed at the CEN laboratory at Saclay, France, and had been used in their original form in previous experiments.⁴⁶ The magnet is documented in Refs. 47–49; we indicate here only the changes that were made at LAMPF prior to the present experiment.

The cryogenic vessel covers were originally sealed with indium gaskets, which experience had shown to be unreli-

able. At the suggestion of the CEN designers, new covers were fabricated and welded in place, resulting in a reliable seal. Liquid helium was fed continuously to the magnet from a 500-l Dewar via a rigid transfer line. The flow was regulated by two cryogenic valves. Isolating the Dewar from the strong fringe field required a transfer line with a length of about 3 m. The consumption of liquid helium was 5.5–6 l/h, of which about 1.5 l/h were consumed in the transfer line.

3. The target refrigerator

The original form of the refrigerator is described in Ref. 50. It was constructed as a ^3He stage with target attached, nested within a ^4He stage, with heat exchange via touch contact through thin-wall stainless steel. For the present experiment, the ^3He stage was mounted on a bellows seal that enabled a few centimeters of vertical movement under cryogenic conditions. This provided adjustment of the target height and proved useful in aligning the target with the beam.

The ^3He pump system consisted of Roots-type blowers backed by a double-stage rotary vane pump. This system had a maximum pumping speed of about 800 l/sec. The ^4He pump system was a rotary vane pump with a speed of about 100 l/sec. A pump of this size was not required, but was used because of its availability. The refrigerator consumed about 2 l/h of liquid helium. The ^3He vapor pressure was measured with a remote-sensing capacitance manometer (MKS Instruments, Inc., Model 310B), the calibration of which was checked by the LANL standards laboratory.

In traversing the target refrigerator, the beam passed through the following total thickness of extraneous materials: PTFE (Teflon), 1.0 mm; copper, 0.25 mm; stainless steel, 0.86 mm; mylar, 0.08 mm; and aluminum, 1.27 mm for the first target and 1.78 mm for the second and third targets.

4. The NMR system

The NMR system operated at a central frequency of 106.5 MHz. The detector, based on real-part detection, was similar to that of Court.⁵¹ The detected signals were processed with a signal averager and transferred to the experimental on-line computer via a CAMAC input gate. The NMR software was a straight integration routine, with an integration range of 640 kHz.

Two NMR coils were present in the target holder; one of them was more sensitive to the target periphery than the other. The polarizations measured with the two coils agreed within uncertainties.

C. Scintillators and wire chambers

The experimental setup used is shown in Fig. 2. The detectors consisted of a set of scintillation counters and multiwire proportional chambers (MWPC's) to define and monitor the beam, a set of scintillation counters to detect the particles scattered by the polarized target over a range of angles near 0° , and MWPC's and scintillation counters used for the C_{LL} measurements. These detectors are

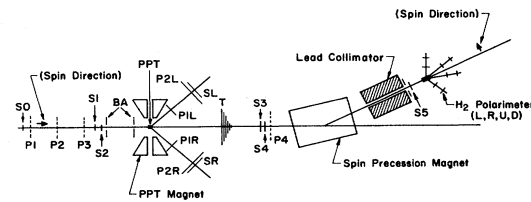


FIG. 2. Diagram of the experimental setup. Scintillation counters are labeled S , veto counters BA , and proportional wire chambers P . The array of transmission counters is labeled T .

described in more detail below. Table I contains the dimensions and location of the detectors in the beam line. The MWPC's were the same ones used at the Argonne ZGS in other polarized-target experiments.^{52–54}

1. Beam detectors

The beam incident on the polarized target was detected in scintillation counters S_0 , S_1 , and S_2 . The counters S_1 and S_2 were segmented into an up-down and a left-right pair, respectively. This permitted monitoring of the beam position as well as a means of rejecting some events with two or more incident particles within the resolving time of the electronics (~ 15 – 20 nsec), as described below. A second set of left-right and up-down scintillation counters (BL , BR , BU , BD) was located downstream of the polarized target; these also monitored the beam position. The combined information from S_1 , S_2 , BL , BR , BU , and BD gave an indication of the incident-beam angle. During normal data-taking periods, the beam was kept centered on each left-right and up-down pair of counters. The MWPC's P_1 , P_2 , P_3 , and P_4 were used to sample the beam trajectories a few times per second to check the beam position and divergence, but they were found to be less sensitive than the scintillation counters to small position changes. We estimate that the worst misalignment of the beam during runs was less than ± 1 mm on the target, and less than $\sim \pm 3$ mr in angle.

TABLE I. Dimensions and positions of detectors in the beam.

Type	Symbol	Thickness (in.)	Size (height \times width) (in.)	Distance from target (in.)
Scintillator	S_0	$\frac{1}{16}$	2×1	-128.5
	$S_1(S_1U, S_1D)$	$\frac{1}{8}$	$\frac{1}{2} \times 1$	-53.5
	$S_2(S_2L, S_2R)$	$\frac{1}{8}$	$1 \times \frac{1}{2}$	-49.5
	BA_1	$\frac{3}{8}$	4×4	-43.5
	BA_2	$\frac{3}{8}$	3×3	-16.5
	$S_3(BU, BD)$	$\frac{1}{4}$	2.5×5	108.6
	$S_4(BL, BR)$	$\frac{1}{4}$	5×2.5	112.9
	BA_3	$\frac{3}{8}$	8×8	~ 280
	S_5	$\frac{1}{4}$	2.75 diam	~ 282
MWPC	P_1		5×5	-119
	P_2		5×5	-92
	P_3		5×5	-65
	P_4		10×20	117.3

The halo-veto counters BA_1 and BA_2 were used to reject beam particles that would miss the polarized target. The fraction of the beam rejected by these counters varied from about 17% at 800 MeV to about 55% at 400 MeV. The diameters of the circular holes in BA_1 and BA_2 were 1.4 cm, whereas the target diameter was 2.0 cm; these holes subtended solid angles of 0.13 and 0.88 msr from the center of the target. The counter BA_1 was viewed by a single photomultiplier, while BA_2 was viewed from opposite sides by two photomultipliers to insure good efficiency. For running at two energies (303 and 620 MeV), P_1 , P_2 , and P_3 were removed from the beam, S_0 was moved 180 cm downstream, and 200 cm of vacuum pipe were installed in the beam to reduce the rejection rate from the BA counters.

Following wire chamber P_4 , the beam was bent and collimated before striking the target in the LH_2 polarimeter.^{39,40} Just upstream of this target was another scintillator S_5 and another veto counter BA_3 with a 7.6-cm-diameter hole which rejected particles that were close to the collimator walls or that might miss the liquid-hydrogen target. The bend was chosen to precess the beam spin direction from purely longitudinal to purely transverse, as described above, so that the beam polarization could be measured. The polarimeter trigger required a signal in S_5 , as well as in S_0 , S_1 , and S_2 , and no signal in BA_1 , BA_2 , or BA_3 .

2. Detectors for the $\Delta\sigma_L$ measurement

The scintillation counters for the $\Delta\sigma_L$ measurements consisted of a set of eleven circular scintillators, each $\frac{1}{4}$ -in. thick, with plastic light guides. These were optically aligned to have a common axis, and they were arranged from largest to smallest diameter in the direction of the beam, to allow for efficiency measurements over most of the acceptance of the counters, as described below. The counters were oriented so that they were perpendicular to the beam and assembled so that there was little overlap of the light guides from the different counters. Each scintillator was viewed by a single EMI 9813B photomultiplier, with the exception of the largest counter, which was viewed from opposite sides by two RCA 8850 photomultipliers. For protection from the field of the polarized target magnet, special magnetic shields were constructed for each photomultiplier.⁵⁵ No effects were observed on the photomultiplier pulse heights as the target field was turned on or off during normal data-taking conditions.

The counters were mounted in a rigid structure on a pair of rails, so the counter assembly could be moved along the beam. The counter axes were optically surveyed to coincide within ± 2 mm with the nominal beamline at any position along the rails. The distance from the polarized target to these counters was adjusted at each beam energy so that the coverage in t , the four-momentum transfer squared (for elastic-scattering kinematics), was approximately the same. In addition, the counter diameters were chosen to give equal increments in t . These scintillation counters were used previously in experiments at LAMPF,⁵⁶⁻⁵⁸ but they are not the ones used in previous $\Delta\sigma_L$ measurements at the Argonne ZGS. The radii of

TABLE II. Radii of the transmission counters.

Counter	Radius (mm)
T_1	228.6
T_2	215.7
T_3	201.7
T_4	186.7
T_5	170.4
T_6	152.4
T_7	132.1
T_8	107.7
T_9	76.2
T_{10}	50.8
T_{11}	25.4

the transmission counters are listed in Table II, and the distances from the center of the polarized target to the first counter T_1 for each energy are listed in Table III. The distance along the beam between corresponding edges of adjacent counters was approximately 2 cm.

3. Detectors for the C_{LL} measurement

A pair of MWPC's on each side of the beam (P_{1L}, P_{2L} and P_{1R}, P_{2R} , as shown in Fig. 2) were used to detect pp elastic-scattering events. The restriction that they be positioned so as not to interfere with the $\Delta\sigma_L$ measurement, together with the limited aperture for scattering allowed by the polarized target magnet, limited the angular coverage to $80^\circ < \theta_{c.m.} < 98^\circ$. The scattered and recoil protons were detected in coincidence. Scintillation counters SL and SR downstream of P_{2L} and P_{2R} were used to define the trigger for the elastic events. Each of these was made up of two counters ($23 \times 5.5 \times 0.5$ in.³), placed side by side. The active area of chambers P_{1L} and P_{1R} was 33.6 cm high by 17.6 cm wide, and of chambers P_{2L} and P_{2R} was 51.2 cm high by 25.6 cm wide. The distance from the polarized target to these chambers was roughly 85 and 148 cm for P_{1R} and P_{2R} , and 99 and 160 cm for P_{1L} and P_{2L} ,

TABLE III. Distances between the center of the polarized target and the first transmission counter T_1 .

T (MeV)	Distance (cm)
302.9	158.2
384.6	158.2
434.4	163.5
485.0	173.4
518.4	180.7
535.4	184.8
569.6	191.2
586.3	195.2
619.8	201.3
636.8	205.4
688.0	215.3
739.5	225.3
790.1	234.8

respectively. The chambers were surveyed in place to within ± 0.4 mm, as indicated by redundant measurements made during the survey.

D. Electronic logic

The basic quantities measured in this experiment were the fractions R_i of the beam transmitted through the target and detected in the transmission counters T_i which subtended solid angles $\Delta\Omega_i$. The information which was used to obtain a value for $\Delta\sigma_L$ was the asymmetry in the R_i associated with the two relative orientations of beam and target polarizations. In order not to have misleading results, it was important to avoid any effects due to counting rates, which could lead to multiple events being counted as single events. This could cause a false asymmetry in counting rates if there were any asymmetry in the beam intensity associated with its spin orientations. (Such asymmetries were generally present during data taking and were sometimes as great as ± 0.1 .) To avoid this problem, several systems of fast logic were used to reject events in which more than a single particle was detected in the beam-defining counters within the resolving time of the fast logic. (The effect of this system was seen, rather dramatically, on one occasion when an unintentional misadjustment of this portion of the logic led to a noticeable lack of reproducibility of the measured values of $\Delta\sigma_L$.) To avoid this problem with the transmission counters, parallel systems of monitoring counter efficiencies and accidental coincidence rates were used. The logic used to identify beam particles is shown in Fig. 3. A BEAM signal was produced by a threefold coincidence of S_0 , S_1 , and S_2 , with a veto from BA_1 or BA_2 . This was,

in turn, vetoed by any signal from one of three sets of logic which were used to identify multiple-beam events, labeled A , B , and C in Fig. 3; a successful beam trigger is labeled TO in that figure. Logic A was a delayed self-coincidence in S_0 which was set to detect any event in which a second pulse occurred in S_0 within 50 nsec of the initial pulse. This system could not respond to two particles so close in time that only a single pulse was seen, but such an event would produce a larger than usual pulse in S_1 or S_2 (as well as in S_0). Logic C was incorporated to detect this class of event. This logic used an alternate set of discriminators on S_1 and S_2 with thresholds set at about 150 mV, where the minimum pulse height of normal beam particles was ~ 100 mV. Logic B used information from the two segments of S_1 and S_2 , which divided the beam area into quadrants, so that it detected events corresponding to counts in more than one of these quadrants. Typically, about 5% of BEAM signals were vetoed by these multiple-event detectors.

In order to form a coincidence between a successful beam event TO and each transmission counter T_i , discriminators with a fast inhibit (equivalent to a strobed coincidence) were used, as shown in Fig. 4. As indicated there, two sets of logic were used to measure the efficiency of each transmission counter and to find the rate of accidental counts. In our notation, counter T_i is upstream of counter T_{i+1} , which is smaller in diameter. The logic shown in Fig. 4 allows one to obtain the efficiency η_i of that portion of T_i shadowed by T_{i+1} and the product $\eta_{i,i+1}$ of similar efficiencies of two adjacent counters T_i and T_{i+1} as follows:

$$\eta_i = T_{i,i+1} / TO_{i+1}$$

and

$$\eta_{i,i+1} \equiv \eta_i \eta_{i+1} = T_{i-(i+3)} / T_{i+2,i+3}$$

where TO_{i+1} is equivalent to a coincidence between the beam signal TO and the counter T_{i+1} ; $T_{i,i+1}$ is

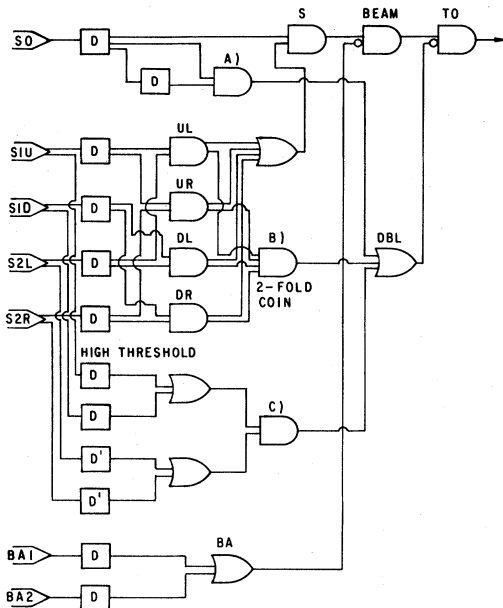


FIG. 3. Diagram of the electronic logic used to identify beam particles. The D 's correspond to discriminators. Three methods of rejecting multiple events are shown in the coincidences A , B , and C , as described in the text.

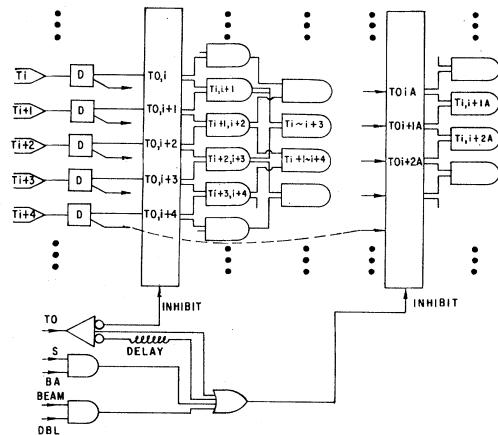


FIG. 4. Diagram of the electronic logic used with the transmission counters T_i . The D 's correspond to discriminators, and the tall rectangles correspond to discriminators with a fast inhibit.

equivalent to a multiple coincidence of TO , T_i , and T_{i+1} ; and $T_{i-(i+3)}$ is equivalent to a multiple coincidence of TO and T_i through T_{i+3} . It should be noted that the efficiencies given by the second method should be less sensitive to accidental coincidence effects. Under normal running conditions (an instantaneous rate of ≤ 300 kHz), both η_i and $\eta_{i,i+1}$ were typically found to be larger than 0.999.

The method used to measure accidental coincidence rates was set up, not with the usual method of delayed coincidence, but with a method which should measure the "true" non-beam-associated accidental rate. This is given approximately by

$$TO_i A(\text{true}) \simeq \frac{2\tau}{t} [T_i - TO_i - (BA \cdot T_i) - (DBL \cdot T_i)] \\ \times (TO - TO_i),$$

where 2τ is the full coincidence width and t is time (including the duty factor of the beam, 9% at 800 MeV and 3% at all other energies).

In this equation, T_i is the singles counting rate in transmission counter i , TO_i represents the coincidence rate between the beam and T_i , $(BA \cdot T_i)$ represents the counting rate in one of the BA counters in coincidence with T_i , and $(DBL \cdot T_i)$ represents the counting rate in the multiple-event detection system described above in coincidence with T_i , so the expression within the square brackets represents the counting rate in T_i not associated with any beam particle. (A large contribution to this signal probably consisted of incident protons which passed through the narrow gap between the two segments of S_1 or S_2 .) The expression within the second set of parentheses represents beam particles that did not produce counts in T_i . The logic setup that was used gave the following "measured" accidental rate:

$$TO_i A(\text{meas}) = \frac{2\tau}{t} [T_i - TO_i - (BA \cdot T_i) - (DBL \cdot T_i)] \cdot TO.$$

A similar one was used for $TO_{i,i+1}A$. The true values were then calculated by multiplying the measured rates by

$$(TO - TO_i)/TO \quad \text{and} \quad (TO - T_{i,i+1})/TO,$$

respectively.

The fraction of beam transmitted through the target R_i was then found from

$$R_i = [T_{i-1,i} - T_{i-1,i}A(\text{true})] / (TO \cdot \eta_{i-1,i})$$

for one set of logic and

$$R_i = [TO_i - TO_i A(\text{true})] / (TO \cdot \eta_i)$$

for the other set. The corrections to $\Delta\sigma_L$ due to the efficiency correction were typically 0.1 to 0.2 mb, and those due to accidental coincidences were much less (~ 0.01 mb). There was no significant difference observed in the resulting calculated asymmetries between the two methods of corrections. The former method was used to obtain the results reported here.

During production runs, the direction of beam polarization was reversed every minute. Scaler data were recorded

on magnetic tape typically every fourth beam pulse (the rate was 120 pulses/sec at 800 MeV and 40 pulses/sec at all other energies), though occasionally they were recorded at every pulse, to allow for later rejection of any anomalous group of beam pulses, as described below.

For the C_{LL} measurement, a coincidence between the BEAM signal described above and the scintillators in the left and right arms gave a trigger to read MWPC data and time-of-flight information (which was not used in the analysis) into the computer. The C_{LL} fast logic was vetoed by a computer busy signal, to allow for independent normalization of these data. Because triggering rates were less than one per pulse, no dead time corrections were necessary. At random intervals, determined by a trigger from a pulser, data from the MWPC's in the beam line were read into the computer for beam profile measurements, and pulse height and timing information from the transmission counters were read into the computer to monitor their gains and timing.

E. Experimental tests

Before beginning data taking, as well as during the course of the experiment, many studies and tests were made to search for any indication of effects associated with the experimental setup or with the experimental procedures used that might lead to false results.

At the start of the experimental run, and whenever there was any change in the beam counters or the target, the alignment of the beam with the veto counters BA_1 and BA_2 and with the target was checked by carefully positioning tungsten rods in the center of the holes in these counters and using the beam to simultaneously photograph these rods and the target holder, forming an image on a piece of high-speed Polaroid film placed directly in the beam. In these pictures, the target support structure was clearly visible, so the position of target and BA counters with respect to the center of intensity of the beam could be determined to $\sim \pm 1$ mm.

An estimate was made of the fraction of the incident beam that missed the target, using the information from the wire proportional chambers in the incident beam. As discussed above, information from these chambers was read into the computer at random intervals, as well as for every C_{LL} event. Samples of several hundred beam tracks, corresponding to each of the two triggers, were studied at two energies, 790 and 385 MeV. (These are the energies of the beam at the center of the target, as determined from machine parameters and energy-loss calculations.) Beam profiles, in both x and y (with y vertical) at the target position were calculated, and the fraction of events with values of x or y greater than ± 1 cm from the center of the target were found to range between 1.0% and 3.5%. No significant difference was noted between the beam tracks from the C_{LL} events and those from the random trigger (which should be the " $\Delta\sigma_L$ " events), or between the two energies. A study was made of those tracks which gave x or y values greater than ± 1 cm from the center of the target. It was found that in 75% of such cases the difference in the slope of the beam as measured between P_1 and P_2 , and between P_2 and P_3 , was found to

correspond to a discrepancy in the calculated position at one chamber greater than a distance of 2.5 wires (0.5 cm). This indicated that a scattering had probably occurred, so that a calculation of the x and y position of these tracks at the target center was unreliable. This indicates that the fraction of the beam missing the target was $\leq 2\%$.

The beam chambers were also used to check the alignment of the polarized target magnet relative to the nominal beam direction. The beam trajectories, before and after the magnet, were observed both with the magnet set at the polarizing field of 2.5 T and with the magnet turned off or set at very low field. The observed deflection at P_4 was 5.3 ± 3.8 mm at 485 MeV, indicating that the magnet was properly aligned to within 0.3° .

The field integral through the polarized target magnet, as well as the calibration of beam energy, was checked with the help of the liquid-hydrogen polarimeter. For this test, the polarimeter was located at a lab angle of 0° centered on the beamline, and the spin-precessing magnet for the polarimeter was turned off. The spin direction of the incident beam was oriented transverse and in the horizontal plane (i.e., S -type), as measured by the EPB polarimeter. The spin direction was measured at the liquid-hydrogen polarimeter both with the polarized target magnet set at the polarizing field and with it turned off. The measured magnet current and spin rotation, the number of turns in the magnet coils, and the beam energy corrected for energy loss to the center of the target were all found to be consistent. If the result of this test is expressed as a measurement of the beam energy, the value found was 474.4 ± 6.0 MeV, whereas the energy from the machine parameters and energy-loss corrections was calculated to be 485.0 MeV, differing by less than two standard deviations. This provides additional confidence that the magnetic field of the polarized target was understood and that the magnetic-field corrections to the outgoing particles in the C_{LL} data were correct.

An estimate was made of the correction to $\Delta\sigma_L$ due to particles scattering backward from the target into the BA_1 and BA_2 counters, which would veto such events. From published pion production cross sections on hydrogen,⁵⁹⁻⁶¹ it was found that the solid angle subtended by these counters at the target could lead to a maximum correction to the measured $\Delta\sigma_L$ values at the highest energies of ± 0.04 mb, and smaller at lower energies. In practice, the correction is expected to be much smaller than this for several reasons: These back-scattered pions were quite low in energy and many would have been stopped in the polarized target; those pions that hit the veto counters would have been quite slow and some would have arrived too late to veto the incident-beam particle signal; and the spin dependence of the pion production cross section is not generally maximal. No corrections to the $\Delta\sigma_L$ data were applied for this effect.

Many tests were also made to check the sensitivity of the measured value of $\Delta\sigma_L$ to various effects associated with the beam and with the target polarization and uniformity. The sensitivity to beam steering was checked by moving the beam horizontally or vertically by distances up to ~ 3 mm (compared with the normal range of beam motion of ~ 0.1 mm). The ratio $T_{9,10}/TO$ should be

most sensitive to these effects; however, no variation in this quantity was seen, within statistical error. The maximum variation observed would correspond to a variation in $\Delta\sigma_L$ of ~ 0.17 mb. These tests also show that the target density was consistent with being uniform, within 0.3%. The sensitivity to possible misalignment of the transmission counters was checked by moving the counters horizontally by distances up to 0.5 in. No effect was seen within the 0.24-mb combined statistical error of these tests. The sensitivity of $\Delta\sigma_L$ to the BA veto counters was checked by removing them from the trigger. The resulting change of $\Delta\sigma_L$ from the average values at that energy (434.4 MeV) was 1.02 ± 0.66 mb.

The sensitivity to N and S polarization components in the beam was checked by running with N - and S -type beams. With an N -type beam at 569.6 and 636.8 MeV, the value of " $\Delta\sigma_L$ " was found to be 2.3 ± 1.4 mb, and with S -type at 485.0 and 619.8 MeV it was found to be -0.18 ± 0.38 mb, both statistically consistent with zero. With an unpolarized target, the value of " $\Delta\sigma_L$ " was found to be 0.00 ± 0.28 mb, as averaged over nearly all energies; similar results were found with an unpolarized beam.

The only experimental condition which we found to affect the value of $\Delta\sigma_L$ was a high beam rate. Tests made over a wide range of rate showed that results were not reproducible if instantaneous beam rates higher than ~ 300 kHz were used. All data were therefore taken at rates lower than this. As discussed below, the errors in experimental values of $\Delta\sigma_L$ used in the final analysis are all consistent with the expected statistical distribution, so there is no indication of rate effects in the results.

III. DATA ANALYSIS

A. $\Delta\sigma_L$

The total-cross-section difference $\Delta\sigma_L(t_i)$ for the i th transmission counter (T_i) was calculated with the formula

$$\Delta\sigma_L(t_i) = \frac{A}{P_T P_B} \ln(R_i^+ / R_i^-) \simeq \frac{2A}{P_B P_T} \epsilon_i,$$

$$\epsilon_i = (R_i^+ - R_i^-) / (R_i^+ + R_i^-),$$

where R_i^\pm is the fraction of the incident protons transmitted through the target and detected with counter T_i for parallel (+) and antiparallel (-) spin states, P_T and P_B are the target and beam polarization, and $A = (N_A \rho L)^{-1}$ is the target constant for free protons, where N_A is Avogadro's number, L is the target length, and ρ is the free proton density. The R_i^\pm were corrected for counter efficiency and accidental coincidences as described above. The symbol t_i denotes the maximum four-momentum transfer squared (for elastic scattering) covered by T_i .

For this experiment to be sensitive to ~ 0.1 mb in $\Delta\sigma_L(t_i)$, the asymmetry (ϵ_i) had to be sensitive to $\sim 10^{-5}$. In order to find any possible systematic effects, several tens of runs, each with statistical errors of ~ 1.5 mb, were made at each energy, about half with each target polarization direction, and correlations between the resulting

values of $\Delta\sigma_L$ and various parameters of the run, such as beam intensity, beam position, etc., were investigated. The only correlation that was found was between $\Delta\sigma_L$ and the product of the beam intensity and its asymmetry. Studies of corrections to $\Delta\sigma_L$ for high-intensity beams with a large asymmetry showed that the largest correction was due to the transmission-counter efficiency. Even after these corrections had been made, as described above, it was noted that the transmission ratio R_i was still somewhat dependent on the beam intensity. The error on the inefficiency ($1-\eta_i$) was estimated to be $\sim 0-20\%$ at ~ 300 -kHz instantaneous rate, depending on the voltage setting of the transmission counters. In order to minimize this effect, the instantaneous beam intensity was kept low (≤ 300 kHz) during data taking, and pulses of high intensity were rejected during off-line beam analysis.

For the replay of the data from tape, the ratio of the doubles in S_0 to the beam counts $S_0(\text{DBL})/C_{\text{beam}}$, with $S_0(\text{DBL})$ as given by logic A described above, was used as an estimator of the instantaneous beam intensity. This quantity was checked with every tape record (every fourth beam pulse, or occasionally every pulse) and the $\Delta\sigma_L$ data for that record were rejected if $S_0(\text{DBL})/C_{\text{beam}}$ exceeded a value corresponding to an instantaneous rate of approximately 1 MHz. After the replay, some runs were rejected if there was any indication that they might have some false asymmetry. The acceptance criteria were the following:

(1) The instantaneous beam intensity, averaged over the run, should be less than 600 kHz.

(2) The asymmetry in $S_0(\text{DBL})/C_{\text{beam}}$, given by

$$\frac{1}{2}[S_0(\text{DBL})/C_{\text{beam}(+)} - S_0(\text{DBL})/C_{\text{beam}(-)}],$$

should be less than $\sim 0.5\%$. This corresponds to the efficiency correction being ≤ 1.5 mb, which means that the maximum error due to the efficiency correction should be ≤ 0.3 mb.

(3) The value of χ^2 for the fit of a straight line to the $\Delta\sigma_L(t_i)$, as discussed below, should be less than 3.0.

Application of these criteria resulted in the rejection of 6% of the runs.

The statistical error of $\Delta\sigma_L(t_i)$ can be written as

$$\delta(\Delta\sigma_L(t_i)) = \frac{2A}{P_B P_T} \left[\frac{1-R_i}{R_i N_0} \right]^{1/2},$$

where N_0 is the number of unambiguously identified incident particles. Since the $\Delta\sigma_L(t_i)$ are not independent of each other, the straight-line fits to $\Delta\sigma_L(t_i)$ were made with the full covariant error matrix,⁵⁷ as described in the Appendix.

The value of $\Delta\sigma_L$ was obtained by extrapolating the $\Delta\sigma_L(t_i)$ to $t=0$ for each run and then taking the weighted average of the $\Delta\sigma_L$ values, or by taking the weighted average of the $\Delta\sigma_L(t_i)$ from the runs and then extrapolating to $t=0$. The two methods gave exactly the same results, as expected. In each method, the $\Delta\sigma_L(t_i)$ were corrected for Coulomb-nuclear interference effects, using the phase shifts of Bhandari, Arndt, Roper, and VerWest,¹¹ before extrapolating. Table IV gives the values of $\Delta\sigma_L(t_i)$ used for the fits, uncorrected for

Coulomb-nuclear interference; they are presented in this manner so that they can be used to evaluate $\Delta\sigma_L$ with different phase shifts or extrapolations.

Various studies were made to determine the appropriate extrapolation to $t=0$. In all cases, the correlated errors were treated as described in the Appendix. It was decided to exclude counter T_2 from the fits, since in two cases (one set of runs each at 485 and 790 MeV) the error on $\Delta\sigma_L(t_i)$ for T_2 was larger than for T_3 . This was caused by efficiency corrections for T_2 that were larger than normal for these two sets of runs, and it led to problems with the correlated error fits. In the interest of consistency, only counters smaller than T_2 were used in the fits, for all energies. It was also found that there was an improvement in the value of χ^2 per degree of freedom (1.68 vs 1.20, averaged over all energies) with a quadratic rather than a linear t dependence when using the Arndt Coulomb-nuclear interference correction.^{11,71} (The linear fit was used, with other Coulomb-nuclear interference corrections, in our earlier paper.²⁷) On the other hand, the values of $\Delta\sigma_L$ obtained either from the linear or quadratic t dependence, using counters T_3-T_9 , T_3-T_{10} , or T_4-T_{10} in the fits, were all identical within statistical uncertainties, in that they differed by less than one standard deviation, except at 570 MeV, where the linear and quadratic fits differed by about two standard deviations. The extrapolation chosen to obtain the final values of $\Delta\sigma_L$ corresponds to the minimum averaged value of χ^2 per degree of freedom, which was the quadratic t dependence with counters T_3-T_9 . The same counters were used with the linear fit in our earlier paper and were also used to obtain values for the slopes $\partial(\Delta\sigma_L)/\partial t$ given below. The final fits are shown in Fig. 5.

At each energy, after the rejection of some runs by the above criteria, the distribution of the values of $\Delta\sigma_L$ from the various runs was investigated to check whether the fluctuations were consistent with statistics. Some sample results of distributions of $\Delta\sigma_L$ are shown in Fig. 6; in every case the agreement with expectation is satisfactory. This indicates that the methods used to find the extrapolated value of $\Delta\sigma_L$ and its error are statistically correct.

The beam polarization used to obtain $\Delta\sigma_L$ for each run was estimated by using the line-B polarimeter, which had high counting rates, giving $\leq 1\%$ error per run, since the counting rates of the LH₂ polarimeter were too low for its results to be used with each run to check the fluctuation of the value of $\Delta\sigma_L$. The results of the LH₂ polarimeter for each energy were used for an additional correction to the beam polarization. In principle, the polarization can be different in the EPB beam line and in line B because of the different phase space of the EPB line, with that of the EPB line expected to be slightly higher, due to the specific features of the Lamb-shift polarized ion source.³³ Because of this, the values of $\Delta\sigma_L$ had to be renormalized by the ratio of the EPB-line polarization to the line-B polarization. By summing up all runs, small uncertainties ($\leq 2\%$) on the EPB polarization as measured by the LH₂ polarimeter were obtained at each energy above 500 MeV, and a correction to $\Delta\sigma_L$ was applied. For these energies, the average value of the ratio of the beam polarization from the two polarimeters was found to be

TABLE IV. Experimental values of the total-cross-section differences $\Delta\sigma_L(t_i)$ for the transmission counters T_i , where t_i is the maximum four-momentum transfer squared for elastic scattering accepted by T_i . The values are not corrected for Coulomb-nuclear interference, and the errors are statistical only.

T_i	T (MeV)	$ t_i $ [(GeV/c) ²]	$\Delta\sigma_L(t_i)$ (mb)	T (MeV)	$ t_i $ [(GeV/c) ²]	$\Delta\sigma_L(t_i)$ (mb)
T_2	302.9	0.0117	-26.35±0.211	384.6	0.0154	-21.21±0.208
T_3		0.0100	-26.65±0.213		0.0132	-21.17±0.211
T_4		0.0084	-26.70±0.216		0.0111	-21.14±0.216
T_5		0.0069	-26.67±0.218		0.0090	-21.02±0.220
T_6		0.0054	-26.81±0.222		0.0071	-20.90±0.224
T_7		0.0039	-26.80±0.226		0.0052	-20.66±0.230
T_8		0.0026	-26.85±0.231		0.0034	-20.60±0.236
T_9		0.0013	-27.11±0.245		0.0017	-20.73±0.249
T_{10}		0.0005	-27.46±0.309		0.0007	-21.19±0.290
T_2	434.4	0.0167	-17.67±0.329	485.0	0.0168	-13.85±0.254
T_3		0.0143	-17.60±0.333		0.0144	-14.04±0.257
T_4		0.0120	-17.37±0.338		0.0121	-13.88±0.262
T_5		0.0098	-17.24±0.345		0.0099	-13.69±0.266
T_6		0.0077	-16.95±0.351		0.0078	-13.45±0.272
T_7		0.0056	-16.75±0.359		0.0057	-13.23±0.278
T_8		0.0037	-16.60±0.369		0.0037	-13.15±0.287
T_9		0.0018	-16.41±0.387		0.0018	-13.02±0.302
T_{10}		0.0008	-16.26±0.438		0.0008	-12.85±0.339
T_2	485.0	0.0169	-14.78±0.433	518.4	0.0170	-11.95±0.200
T_3		0.0144	-14.80±0.425		0.0146	-11.88±0.203
T_4		0.0121	-14.58±0.433		0.0123	-11.68±0.206
T_5		0.0099	-14.50±0.441		0.0100	-11.48±0.210
T_6		0.0078	-14.15±0.451		0.0079	-11.24±0.214
T_7		0.0057	-13.83±0.461		0.0058	-11.01±0.219
T_8		0.0037	-13.64±0.475		0.0038	-10.85±0.225
T_9		0.0018	-13.47±0.498		0.0019	-10.69±0.236
T_{10}		0.0008	-13.65±0.564		0.0008	-10.75±0.266
T_2	535.4	0.0169	-12.42±0.299	535.4	0.0169	-11.44±0.223
T_3		0.0145	-12.30±0.302		0.0145	-11.59±0.226
T_4		0.0122	-12.07±0.308		0.0122	-11.41±0.229
T_5		0.0100	-11.82±0.314		0.0100	-11.18±0.234
T_6		0.0078	-11.55±0.320		0.0078	-11.01±0.238
T_7		0.0058	-11.22±0.326		0.0058	-10.84±0.244
T_8		0.0038	-11.13±0.336		0.0038	-10.77±0.251
T_9		0.0019	-11.10±0.352		0.0019	-10.67±0.264
T_{10}		0.0008	-11.48±0.394		0.0008	-10.77±0.295
T_2	569.6	0.0171	-11.06±0.162	586.3	0.0170	-11.63±0.222
T_3		0.0147	-11.00±0.164		0.0146	-11.66±0.225
T_4		0.0123	-10.88±0.166		0.0123	-11.51±0.229
T_5		0.0101	-10.79±0.170		0.0101	-11.42±0.223
T_6		0.0079	-10.54±0.173		0.0079	-11.25±0.238
T_7		0.0059	-10.34±0.177		0.0058	-11.11±0.244
T_8		0.0038	-10.11±0.182		0.0038	-10.97±0.251
T_9		0.0019	-9.96±0.191		0.0019	-10.76±0.263
T_{10}		0.0008	-9.78±0.212		0.0008	-10.65±0.292
T_2	619.8	0.0172	-12.23±0.196	636.8	0.0171	-12.34±0.244
T_3		0.0147	-12.47±0.198		0.0147	-12.39±0.246
T_4		0.0124	-12.42±0.202		0.0124	-12.43±0.251
T_5		0.0102	-12.42±0.205		0.0101	-12.43±0.255
T_6		0.0080	-12.31±0.210		0.0080	-12.38±0.260
T_7		0.0059	-12.20±0.214		0.0059	-12.25±0.266
T_8		0.0038	-12.24±0.221		0.0038	-12.24±0.273
T_9		0.0019	-12.25±0.231		0.0019	-12.18±0.286
T_{10}		0.0008	-12.23±0.256		0.0008	-12.17±0.316

TABLE IV. (Continued).

T_i	T (MeV)	$ t_i $ [(GeV/c) ²]	$\Delta\sigma_L(t_i)$ (mb)	T (MeV)	$ t_i $ [(GeV/c) ²]	$\Delta\sigma_L(t_i)$ (mb)
T_2	688.0	0.0172	-15.24±0.122	739.5	0.0172	-16.40±0.109
T_3		0.0148	-15.35±0.123		0.0148	-16.56±0.110
T_4		0.0124	-15.47±0.125		0.0125	-16.71±0.112
T_5		0.0102	-15.56±0.127		0.0102	-16.86±0.114
T_6		0.0080	-15.65±0.130		0.0081	-17.00±0.116
T_7		0.0059	-15.72±0.133		0.0060	-17.10±0.118
T_8		0.0039	-15.78±0.137		0.0039	-17.25±0.122
T_9		0.0019	-15.94±0.143		0.0019	-17.40±0.127
T_{10}		0.0008	-16.17±0.157		0.0008	-17.53±0.138
T_2	790.1	0.0173	-14.82±0.292	790.1	0.0173	-16.32±0.182
T_3		0.0149	-15.30±0.291		0.0149	-16.53±0.184
T_4		0.0126	-15.42±0.298		0.0126	-16.65±0.187
T_5		0.0103	-15.63±0.302		0.0103	-16.75±0.190
T_6		0.0081	-15.85±0.306		0.0081	-16.96±0.194
T_7		0.0060	-15.97±0.314		0.0060	-17.11±0.199
T_8		0.0039	-16.10±0.321		0.0039	-17.26±0.204
T_9		0.0019	-16.29±0.337		0.0019	-17.45±0.214
T_{10}		0.0009	-16.10±0.364		0.0009	-17.68±0.233

$$P_B(\text{line B})/P_B(\text{LH}_2)=0.975\pm 0.020.$$

Below 500 MeV, this average ratio was used to estimate the EPB-line polarization using the data from the line-B polarimeter, because of poor statistics with the LH₂ polarimeter. The uncertainty of the beam polarization ($\sim 2\%$) was due to the statistical error from the LH₂ polarimeter (above 500 MeV) or to the standard deviation of the ratio (below 500 MeV), together with the uncertainty of the calibration of the polarimeter by the quench measurement ($\sim 1\%$).^{36,37} The results of the calibration of the analyzing power of the LH₂ polarimeter are shown in Fig. 7.

Three different sets of target beads were used during the five months of the measurement. The 485- and 790-MeV data were taken with the first target, the 385-, 535-, and 637-MeV data were taken with the second, and the remainder were taken with the third. At 485, 535, and

790 MeV, measurements of $\Delta\sigma_L$ were repeated with the third target. The target polarizations and target constants of the first and second target were normalized to the third one to separate the overall normalization uncertainty.

The target polarization was found from

$$P_T = C_{\text{NMR}} \int S_{\text{NMR}}(P),$$

where $\int S_{\text{NMR}}(P)$ designates the integral of the enhanced (polarized) NMR signal. C_{NMR} is a constant which was found from thermal-equilibrium (TE) measurements by

$$C_{\text{NMR}} = NP_{\text{TE}} / \int S_{\text{NMR}}(\text{TE}),$$

$$P_{\text{TE}} = \tanh(\mu B / kT_{\text{TE}}),$$

where P_{TE} is the polarization at thermal equilibrium, N is

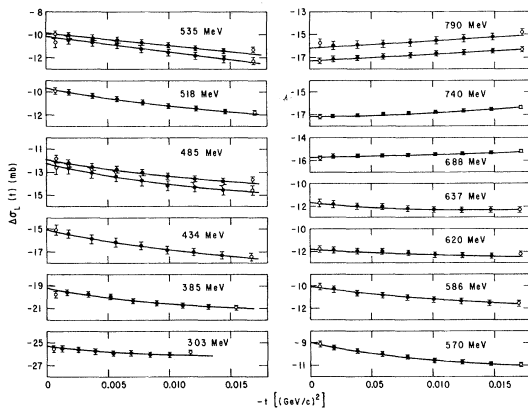


FIG. 5. The quadratic fits to the experimental values of $\Delta\sigma_L(t_i)$ vs t which were used to find $\Delta\sigma_L$. The errors shown are statistical only.

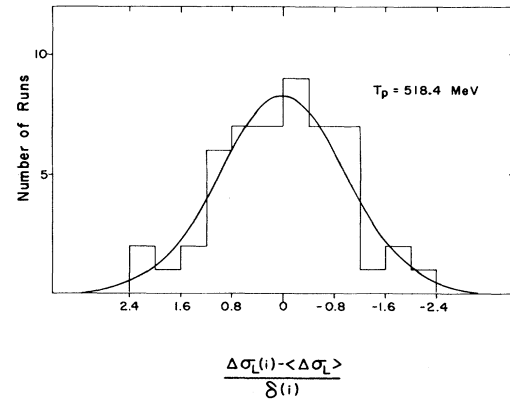


FIG. 6. An example of the distribution of values of $\Delta\sigma_L$ for various experimental runs at 518.4 MeV. The quantity plotted is the difference between the individual experimental value and the average, divided by the estimated error on that value; the curve shown is that of a normal distribution.

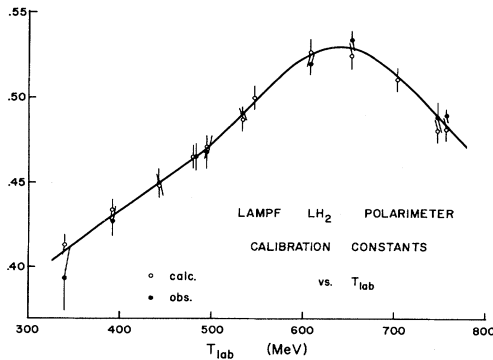


FIG. 7. Comparison of the calculated and observed calibration constants for the LH_2 polarimeter. The calculated values were obtained from a global fit to pp elastic polarization data averaged over the LH_2 -polarimeter acceptance (Refs. 39 and 40) and corrected for background. The observed values were obtained from quench information, as described in the text.

the ratio of the amplifier gain and the number of signal-averager sweeps of the enhanced signal and the TE signal, μ is the proton magnetic moment, B is the magnetic field, which is accurately known from the central NMR frequency, k is Boltzmann's constant, and T_{TE} is the temperature of the target (~ 1 K), which was estimated from the vapor pressure of the ^3He . Thermal-equilibrium measurements were performed 5 times for the first target, 8 times for the second, and 22 times for the third. Average values of the C_{NMR} were obtained for each target. The standard deviation of each set of measurements was considered to be an estimator of the relative uncertainty of the C_{NMR} of each target. The maximum absolute target polarizations for each set of runs are summarized in Table V. For the second target, the value of C_{NMR} was $\sim 10\%$ smaller than that of the other two, owing to water condensation on the NMR coil. C_{NMR} for the second target was renormalized so that the average of the maximum target polarization for the second target was the same as that of the third.

The target constants were also different for the three targets. The ratio of the target constants was estimated from transmission ratios (T_{23}/TO , T_{45}/TO , and T_{67}/TO). The ratio of the attenuation of beam particles by the target beads and other materials that the beam passed through was calculated, assuming that the total cross section is proportional to $A_N^{2/3}$, where A_N is the nuclear atomic weight. The values found for these ratios and used in the computation of $\Delta\sigma_L$ were

$$A(1\text{st})/A(3\text{rd})=1.025\pm 0.008$$

and

$$A(2\text{nd})/A(3\text{rd})=1.014\pm 0.005.$$

These values are consistent with the target-weight measurements, although the accuracy is poor because, unfortunately, some amount of material was lost during removal of the first two targets.

No corrections were made for possible effects of polar-

TABLE V. Maximum values of the target polarization (values of P_{max} in parentheses correspond to raw polarizations with water condensation on the NMR coil).

T (MeV)	Target	P_{max}
485.0	1st	0.842
790.1	1st	0.821
535.4	2nd	0.838 (0.749)
384.6	2nd	0.839 (0.750)
636.8	2nd	0.832 (0.743)
434.4	3rd	0.827
586.3	3rd	0.839
688.0	3rd	0.844
739.5	3rd	0.832
569.6	3rd	0.836
518.4	3rd	0.834
790.1	3rd	0.840
485.0	3rd	0.838
535.4	3rd	0.842
619.8	3rd	0.832
302.9	3rd	0.833
Average		0.836 ± 0.006

ized nuclei, such as ^{13}C , ^{17}O , or ^2H , on the $\Delta\sigma_L(pp)$ measurements. On the basis of natural abundances, the largest effect would be expected from ^{13}C . In the worst case, assuming equal spin temperatures for ^1H and ^{13}C in the polarized target and

$$\Delta\sigma_L(p^{13}\text{C})=2\sigma_{\text{tot}}(p^{13}\text{C}),$$

the effect of polarized ^{13}C on the measured value of $\Delta\sigma_L(pp)$ could be as large as 15%. Based on guidance from $\Delta\sigma_L(pd)$ measurements,⁶² a more realistic estimate would give an effect of 2% or less. Since information on $\Delta\sigma_L(p^{13}\text{C})$ and on the polarization of ^{13}C in the target was lacking, no correction for this effect was applied.

The overall normalization uncertainty (one standard deviation) is estimated to be 4.1%. It is due principally to the uncertainty in the normalization of the target polarization and to the uncertainty in the target constant. The target-polarization normalization uncertainty is 2.1%, comprising the standard deviation of the TE measurements for the third target (1.5%), the uncertainty of the temperature (1.0%), and the possible nonlinearity of the NMR amplifier (1.0%). The beads of the third target were weighed after the experiment (13.09 ± 0.04 g), and chemical analyses were made to obtain the weight of the hydrogen (1.288 ± 0.020 g). The diameter of the target container (2.031 ± 0.014 cm) was measured at liquid-nitrogen temperature when the target beads were loaded. Thermal shrinkage between liquid-nitrogen and liquid-helium temperatures is expected to be negligible ($< 0.3\%$). The uncertainty of the target constant was 3.5%, comprising the uncertainty of the chemical analysis (1.5%), the cross section of the target container (1.4%), the mass of the third target (0.3%), the boundary effects on the packing fraction (1.5%), and the reproducibility of the packing fraction (2.4%), which is estimated from bench-top trial packings of target beads. This last source

of uncertainty has been applied uniformly, although it actually applies only to the first and second targets, for which reliable weight measurements were not obtained. The quoted uncertainty is a conservative overestimate for the third target.

The uncertainty in packing fraction (or density) owing to boundary effects is an allowance for possible effects of the target container walls in estimating the effective (beam-sampled) target density. There are two boundary effects, of opposite sign, which tend to nullify each other if only a limited "core" region of the target is illuminated by the beam. Both effects occur whenever the target vessel walls are essentially planar and the target beads have a uniform size. The first effect arises from the circumstance that there are no "fractional" target beads available to fill the extra empty space induced at the walls of the target vessel. This "boundary-volume excess" (BVE) is reasonably well characterized⁶³ both theoretically and empirically and amounts to 2–3% for a target of our dimensions. The second effect, which we may call the "boundary-induced regularity" (BIR), originates in the ability of a smooth wall to induce regular close packing, as opposed to random close packing, in the first few layers of beads adjacent to the wall.^{64,65} In actual targets contained in transparent vessels, evidence suggestive of BIR is usually seen. Regular packing achieves a higher packing fraction (~ 0.74) than random packing (~ 0.64), so it tends to lead, in effect, to a volume deficit at the target periphery compared to the interior, an effect opposite to that of the BVE. In the general case it is difficult to estimate the net influence of the two effects. In a "worst-case" scenario, one could imagine that the target consists of a regular-packed outer annulus, not sampled by the beam, and a loose-packed, beam-sampled core. In this scenario the interior density could be as much as 12% less than the measured mean density, since the minimal stable packing fraction for so-called "loose random packing" is around⁶⁴ 0.57. For our real target, several considerations argue that the departure from the measured mean value must be much less than this: (a) the experimental tests described in Sec. II E give no indication of a large nonuniformity of the target constant; (b) in practice, it requires some deliberate effort to achieve packing fractions approaching values as low as 0.57, whereas in packing a real target the opposite effort is made, that is, to maximize the packing; and (c) perhaps most important, the radius of curvature of our target vessel walls was only ten times the target bead radius. Both geometrical intuition and information from the available literature⁶⁶ suggest that an appreciable annulus of BIR is not possible in such a relatively small container. In fact, the data of Ref. 66 imply that the BVE dominates the BIR for radial ratios as small as 10. Nevertheless, since an explicit correction factor for the boundary effects seems elusive, we have retained the measured mean density in estimating the third target constant and assigned a further uncertainty of 1.5% (about one-half of the maximal BVE effect) to the packing fraction. We believe that this represents realistic one-standard-deviation limits on the boundary effects.

The final experimental values of $\Delta\sigma_L$ are shown in Fig. 8 and summarized in Table VI, together with errors and

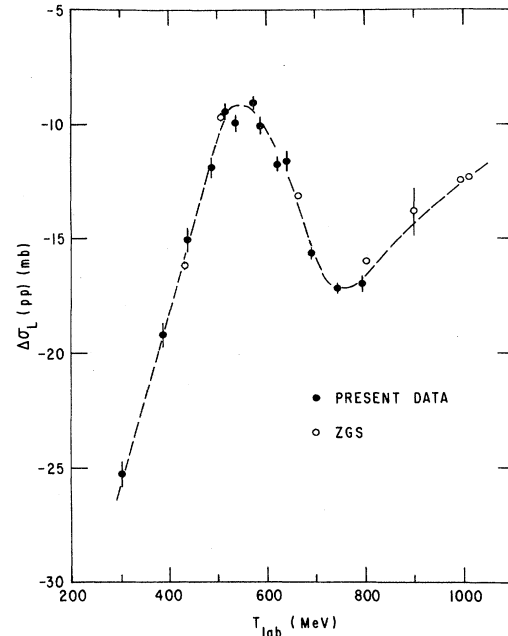


FIG. 8. The experimental values of $\Delta\sigma_L$, together with previous values found at the ZGS (Ref. 1). The errors shown are statistical only.

other quantities of interest. The errors in the table include statistical errors from the fitting procedure and uncertainties from the beam polarization measurements and from the ratios of the target constants discussed above. The experimental values of the slope $\partial(\Delta\sigma_L)/\partial t$, without Coulomb corrections, are shown in Fig. 9 and listed in Table VII. The systematic errors are summarized in Table VIII.

B. C_{LL}

The spin-correlation parameter $C_{LL}(\theta)$ was calculated for each run with the formula

$$C_{LL}(\theta) = \frac{1}{P_B P_T} \frac{I^+(\theta) - I^-(\theta)}{I^+(\theta) + I^-(\theta)},$$

where $I^\pm(\theta)$ is the intensity of elastic pp scattering at a center-of-mass angle θ for parallel (+) and antiparallel (−) spin states, and P_T and P_B are the target and beam polarization. As discussed above, the elastic events used to determine C_{LL} were detected in MWPC's placed on each side of the beam. The MWPC's covered a center-of-mass angular region near 90° and were triggered by signals from scintillation counters placed after them, in coincidence with a beam signal. These events were separated from background by a series of tests on the trajectories of the scattered and recoil protons as reconstructed from the position information taken from the MWPC's. The methods used are outlined below; a more detailed description is given elsewhere.⁶⁷

In order to reconstruct these tracks, it was necessary to

TABLE VI. Experimental values of $\Delta\sigma_L$, resulting from extrapolating the $\Delta\sigma_L(t_i)$ to $t=0$, using counters T_3 through T_9 , assuming a quadratic t dependence. Results are given for data both corrected and uncorrected for Coulomb-nuclear interference, listed as $\Delta\sigma_L(\text{uncorr})$ and $\Delta\sigma_L(\text{corr})$, so that the size of the correction can be seen. The first error on $\Delta\sigma_L$ corresponds to the statistical uncertainty from the fit, and the second error combines the statistical uncertainty with the energy-dependent uncertainties due to the beam polarization and target constant. There is an additional normalization uncertainty of $\pm 4.1\%$, as described in the text. The value of χ^2 per degree of freedom for the fit is listed as χ_a^2 , and the value of χ^2 per degree of freedom for the deviations of the runs from the weighted average of all runs is listed as χ_b^2 . The total number of runs used to obtain $\Delta\sigma_L$ at each energy is listed as N .

T (MeV)	$\Delta\sigma_L(\text{uncorr})$ (mb)	$\Delta\sigma_L(\text{corr})$ (mb)	χ_a^2	χ_b^2	N
302.9	$-27.04 \pm 0.26 \pm 0.59$	$-25.31 \pm 0.26 \pm 0.59$	3.48	1.17	34
384.6	$-20.51 \pm 0.27 \pm 0.54$	$-19.23 \pm 0.27 \pm 0.54$	2.67	1.02	36
434.4	$-16.20 \pm 0.41 \pm 0.54$	$-15.11 \pm 0.41 \pm 0.54$	0.89	0.46	19
485.0	$-12.82 \pm 0.32 \pm 0.47$	$-11.91 \pm 0.32 \pm 0.47$	0.69	0.89	23
485.0	$-13.15 \pm 0.54 \pm 0.59$	$-12.23 \pm 0.54 \pm 0.59$	1.24	0.38	8
518.4	$-10.47 \pm 0.25 \pm 0.34$	$-9.69 \pm 0.25 \pm 0.34$	0.24	0.97	52
535.4	$-10.82 \pm 0.38 \pm 0.44$	$-10.10 \pm 0.38 \pm 0.44$	1.46	0.79	24
535.4	$-10.58 \pm 0.28 \pm 0.36$	$-9.87 \pm 0.28 \pm 0.36$	0.59	1.30	29
569.6	$-9.64 \pm 0.21 \pm 0.26$	$-9.06 \pm 0.21 \pm 0.26$	2.43	0.91	55
586.3	$-10.62 \pm 0.28 \pm 0.37$	$-10.09 \pm 0.28 \pm 0.37$	0.77	1.22	27
619.8	$-12.18 \pm 0.25 \pm 0.32$	$-11.77 \pm 0.25 \pm 0.32$	2.10	1.09	25
636.8	$-12.04 \pm 0.31 \pm 0.43$	$-11.65 \pm 0.31 \pm 0.43$	0.73	1.24	21
688.0	$-15.98 \pm 0.15 \pm 0.27$	$-15.66 \pm 0.15 \pm 0.27$	0.74	1.57	32
739.5	$-17.49 \pm 0.14 \pm 0.24$	$-17.17 \pm 0.14 \pm 0.24$	0.43	1.13	40
790.1	$-16.51 \pm 0.36 \pm 0.57$	$-16.15 \pm 0.36 \pm 0.57$	0.86	2.13	11
790.1	$-17.63 \pm 0.23 \pm 0.33$	$-17.27 \pm 0.23 \pm 0.33$	0.95	1.42	50

correct for the effect of the 2.5-T axial magnetic field which surrounded the target. The method used involved generating pp elastic-scattering events which simulated the real events, using Monte Carlo methods, tracing them through the magnetic field, and finding their coordinates in the MWPC's. Once a set of such events was generated,

the chamber coordinates were used to make a least-squares fit to the coefficients of a linear polynomial relating the chamber coordinates to corrections due to the magnetic field for various geometrical parameters, such as the coordinates of the track on a plane passing through

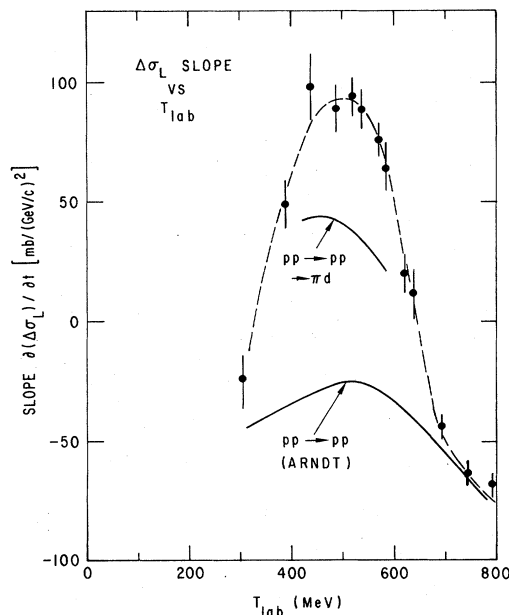


FIG. 9. The experimental values of the slope $\partial(\Delta\sigma_L)/\partial t$, without Coulomb corrections. The errors shown are statistical only. The curves are discussed in Sec. IV B.

TABLE VII. Experimental values of the slope $\partial(\Delta\sigma_L)/\partial t$, resulting from a linear fit to the $\Delta\sigma_L(t_i)$, uncorrected for Coulomb-nuclear interference, using counters T_3 through T_9 . The quoted errors are statistical only. Weighted averages of the two sets of runs at 485, 535, and 790 MeV are also given. The units are $\text{mb}/(\text{GeV}/c)^2$.

T (MeV)	$\partial(\Delta\sigma_L)/\partial t$	Average
302.9	-25 ± 11	
384.6	49 ± 10	
434.4	98 ± 14	
485.0	84 ± 11	
		89 ± 10
518.4	102 ± 18	
535.4	94 ± 8	
	108 ± 13	
		89 ± 8
569.6	78 ± 9	
586.3	76 ± 7	
619.8	65 ± 10	
636.8	20 ± 8	
688.0	12 ± 10	
739.5	-44 ± 5	
790.1	-63 ± 5	
	-80 ± 12	
		-69 ± 6
	-65 ± 8	

TABLE VIII. Systematic errors on the values of $\Delta\sigma_L$ (one standard deviation).

Target polarization		2.1%
Reproducibility of TE	1.5%	
Temperature	1.0%	
Nonlinearity	1.0%	
Target constant		3.5%
Chemical analysis	1.5%	
Area of the container	1.4%	
Mass of third target	0.3%	
Reproducibility of packing fraction	2.4%	
Boundary effects on packing fraction	1.5%	
Total		4.1%

the center of the target and the polar and azimuthal angles θ and ϕ of the track. These fitted coefficients were later used with the real events to reconstruct these same quantities. Two independent methods were used to trace the proton trajectories through the magnetic field, as a check; the agreement between the two was good to $\leq 0.1\%$. For the Monte Carlo events, the difference between the generated (true) values of the parameters and their reconstructed values was $\sim \pm 0.2^\circ$ in θ , $\sim \pm 0.7^\circ$ in ϕ , $\sim \pm 0.7$ mm in y_0 , and $\sim \pm 1.5$ mm in z_0 , where y_0 and z_0 are the coordinates of the track on the $x=0$ plane in a coordinate system centered in the target with z along the beam, y up, and x defined for a right-handed system.

All events which had one and only one hit in each of the four MWPC's were taken to be candidates for pp scattering. In each case, the two tracks were reconstructed, corrected for magnetic-field effects, and the following quantities were calculated: the distance of closest approach (DCA) of the tracks, the coordinates of the interaction point (x_T, y_T, z_T) , taken to be the midpoint of the line between the points of closest approach on the tracks, the difference in azimuthal angle $\Delta\phi$ between the tracks, and the sum of the polar angles of the left and right tracks $(\theta_L + \theta_R)_{c.m.}$ in the center-of-mass system, assuming the kinematics of elastic scattering. After some study, fairly loose cuts were made on all of these quantities except $\Delta\phi$, which was used to make the final background subtraction. The cuts on x_T , y_T , and z_T corresponded to requiring that the interaction take place inside the target and the cut on $(\theta_L + \theta_R)_{c.m.}$ corresponded to requiring that this sum be consistent with 180° . The values of θ_L and $\theta_R(c.m.)$ were used to bin the events by center-of-mass angle, using the average of the value of θ (c.m.) as found from each track. For each of these 2° angular bins, a histogram of $\Delta\phi$ was made, which always exhibited a well-defined peak around 180° , with a background that was never greater than $\sim 5\%$ of the peak height. An example of one of these distributions is shown in Fig. 10. For each of these, the number of events was found by fitting a straight line to the background on each side of the peak and subtracting the number of calculated background events from the total number of events in the peak. This was done separately for each angular bin in

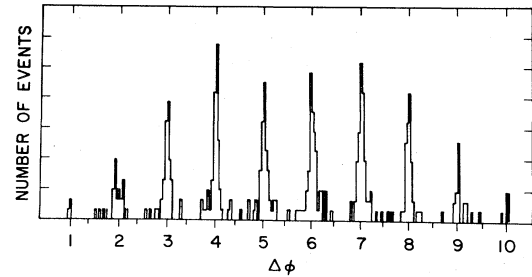


FIG. 10. Typical set of histograms of $\delta\phi$ for the C_{LL} data for a single run. The marks indicate the position of $\delta\phi = 180^\circ$ for each peak. Mark No. 1 is for events between 79° and 81° c.m., and the other marks are for angular bins increasing by 2° . The vertical scale runs from zero to 31 counts.

each run at each energy. The value of $C_{LL}(\theta)$ was then found from the expression above, where I^\pm was taken to be the number of elastic events detected divided by the number of incident beam particles for that run, and P_B and P_T were the beam and target polarizations found for that run, as discussed above.

The values of C_{LL} thus found for each run at each energy and in each angular bin were combined to give a weighted average of $C_{LL}(\theta)$ for each energy and each 2° angular bin, for angles between 80° and 98° . The statistical quality of the results were studied with χ^2 tests. Those runs with large deviations were examined, and some were discarded, but only when reasons other than a large χ^2 value were found to reject them. A test of the χ^2 distribution of the full set of $C_{LL}(\theta)$ data were also performed. Since the number of degrees of freedom was not constant over the data set, a histogram was made of the quantity

$$y_2 = (2\chi^2)^{1/2} - (2n_D - 1)^{1/2},$$

where n_D is the number of degrees of freedom, which should be normally distributed with unit standard deviation.⁶⁸ The distribution was found skewed toward negative values, however, but when all errors were reduced by 10%, the resulting distribution was consistent with expectation. On the basis of this, all errors on the final C_{LL} values were reduced by 10%. It is believed that the source of this apparent overestimate of error was the method used to calculate errors in the computer program which fitted a background under the peak in the $\Delta\phi$ distribution. The final distribution of y_2 is shown in Fig. 11.

The resulting values of $C_{LL}(\theta)$ were fitted at each energy to a curve of the form

$$C_{LL}(\theta) = \alpha + \beta \cos^2\theta,$$

which reflects the expected symmetry around 90° . The values of χ^2 for each fit at each energy were satisfactory. The values of $C_{LL}(\theta)$, with the fitted curve, are shown in Fig. 12 and tabulated in Table IX, with their statistical errors. The systematic uncertainties, due to uncertainties in the beam and target polarization, are $\pm 2.0\%$ and $\pm 2.1\%$, respectively, as discussed above. Values of $\alpha = C_{LL}(90^\circ)$ are plotted in Fig. 13 and tabulated in Table X. Also shown in Fig. 13 are the values of C_{LL} found previously

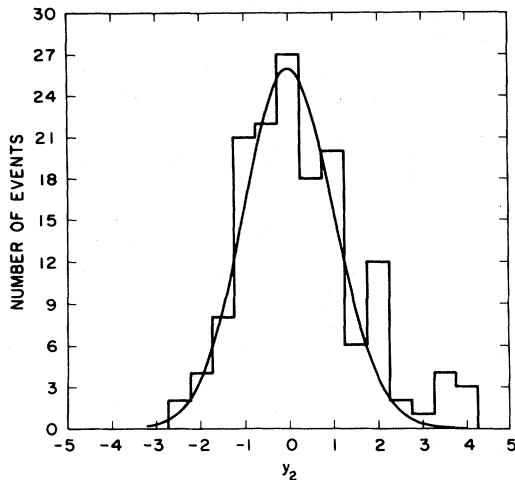


FIG. 11. Distribution of the quantity y_2 described in the text. The curve shown is that of a normal distribution.

at the ZGS.²⁶ We note that the value of the ZGS point near 560 MeV is in doubt, since it now appears that it suffered from beam depolarization effects which had not been taken into account. Values of β are also tabulated in Table X. As can be seen, the errors in this quantity are fairly large, due to the limited angular range of the data.

As an additional check on the validity of these results, a measurement was made of the quantity $C_{SL}(\theta)$ at 485 MeV, with the beam set for S -type polarization. The data were analyzed as described above, and the value for $\theta_{c.m.}=90^\circ$, which should be zero, was found to be (0.0158 ± 0.0188) , consistent with zero. When the $C_{SL}(\theta)$ were fitted to a curve of the form

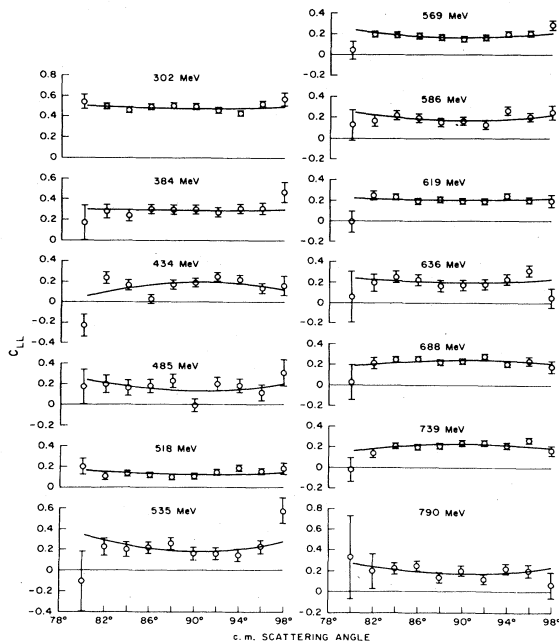


FIG. 12. The experimental values of C_{LL} , with the curves fitted to $\alpha + \beta \cos^2\theta$. The errors shown are statistical only.

$$C_{SL}(\theta) = \gamma \cos\theta,$$

the value of γ was found to be (0.71 ± 0.24) , with χ^2 per degree of freedom equal to 0.65. The value of γ predicted by the phase shifts of Arndt *et al.*⁷¹ (solution WI82) is 0.17. The experimental values of C_{SL} are tabulated in Table XI.

C. Comparison of the $\Delta\sigma_L$ results with other data

Figure 14 shows a comparison of the $\Delta\sigma_L$ results from this work with previous values from the ZGS,¹ from the BASQUE group at TRIUMF³⁰ and from the Geneva group at SIN.²⁹ The data are shown both with statistical uncertainties only and with combined systematic and statistical uncertainties. The agreement with the ZGS and the preliminary SIN results is good except for one or two points, but there is a sizable discrepancy with the TRIUMF data.

The ZGS $\Delta\sigma_L$ data were taken in two different runs separated by about a year. It is possible that there was a systematic difference in the target constant or the target polarization for the two ZGS runs. To indicate this, the ZGS $\Delta\sigma_L$ data in Fig. 14 are shown with two different symbols. The systematic uncertainties on each set of data are roughly $\pm 8\%$.

After these data were published, more and more evidence was found for beam depolarization effects at the ZGS, even at low momenta. Such a depolarization would lead to $\Delta\sigma_L$ values whose magnitudes are too small. This was especially true at 561 MeV, where effects of up to 25% were detected in the beam polarization. A higher-order depolarizing resonance in the ZGS was found close to this energy three years after the $\Delta\sigma_L$ data were taken.⁶⁹

A study of beam polarization at the ZGS has recently been completed.⁴⁰ This study utilized evidence from many sources and from several polarimeters, including the one described in this paper. The ZGS $\Delta\sigma_L$ data had been normalized to P_B results from the 50-MeV polarimeter, which was located between the polarized ion source and injection into the ZGS. However, the evidence from Ref. 40 suggests that the 50-MeV polarimeter calibration constant was too small by roughly 8%. This effect is in the

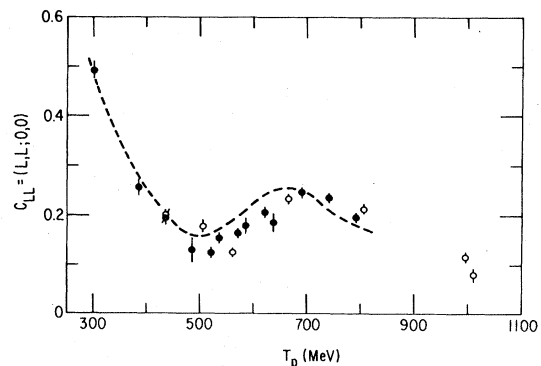


FIG. 13. The experimental values of $C_{LL}(90^\circ)$ (closed circles), with the previous data of Ref. 26 (open circles). The errors shown are statistical only. The curve is a prediction of the phase shifts of Bhandari, Arndt, Roper, and VerWest (Ref. 11).

TABLE IX. Experimental values of $C_{LL}(\theta)$. (There is an additional normalization uncertainty of $\pm 2.0\%$ at each energy on these results due to beam-polarization uncertainty and an overall normalization uncertainty of $\pm 2.1\%$ due to target-polarization uncertainty.)

$\theta_{c.m.}$	T (MeV)	C_{LL}	T (MeV)	C_{LL}
80°	302.9	0.540±0.069	384.6	0.164±0.173
82°		0.496±0.032		0.278±0.066
84°		0.457±0.022		0.233±0.051
86°		0.488±0.019		0.293±0.041
88°		0.502±0.018		0.292±0.039
90°		0.491±0.017		0.292±0.039
92°		0.460±0.018		0.267±0.039
94°		0.427±0.021		0.301±0.042
96°		0.518±0.028		0.302±0.053
98°		0.565±0.064		0.461±0.098
80°	434.4	-0.233±0.110	485.0	0.169±0.169
82°		0.238±0.056		0.195±0.086
84°		0.169±0.045		0.158±0.074
86°		0.029±0.042		0.176±0.064
88°		0.176±0.038		0.227±0.062
90°		0.192±0.038		-0.011±0.059
92°		0.250±0.038		0.197±0.067
94°		0.220±0.040		0.179±0.065
96°		0.132±0.049		0.111±0.075
98°		0.159±0.096		0.307±0.128
80°	518.4	0.199±0.078	535.4	-0.118±0.291
82°		0.106±0.030		0.219±0.080
84°		0.133±0.024		0.195±0.072
86°		0.116±0.022		0.208±0.057
88°		0.098±0.021		0.254±0.054
90°		0.107±0.022		0.153±0.057
92°		0.145±0.022		0.150±0.057
94°		0.185±0.023		0.136±0.063
96°		0.155±0.027		0.221±0.065
98°		0.185±0.050		0.565±0.109
80°	569.6	0.041±0.082	586.3	0.135±0.145
82°		0.196±0.027		0.176±0.052
84°		0.188±0.021		0.227±0.038
86°		0.178±0.019		0.201±0.037
88°		0.165±0.019		0.159±0.034
90°		0.150±0.019		0.170±0.034
92°		0.165±0.020		0.136±0.035
94°		0.194±0.020		0.272±0.035
96°		0.201±0.022		0.209±0.039
98°		0.288±0.040		0.255±0.066
80°	619.8	-0.010±0.102	636.8	0.059±0.252
82°		0.250±0.037		0.199±0.083
84°		0.233±0.026		0.256±0.055
86°		0.191±0.025		0.228±0.055
88°		0.206±0.024		0.171±0.050
90°		0.192±0.024		0.181±0.046
92°		0.189±0.025		0.183±0.048
94°		0.241±0.026		0.240±0.048
96°		0.197±0.030		0.323±0.055
98°		0.190±0.059		0.051±0.098

TABLE IX. (Continued).

$\theta_{c.m.}$	T (MeV)	C_{LL}	T (MeV)	C_{LL}
80°	688.0	0.023±0.172	739.5	-0.022±0.121
82°		0.210±0.054		0.142±0.037
84°		0.246±0.030		0.213±0.018
86°		0.250±0.026		0.204±0.015
88°		0.219±0.027		0.216±0.015
90°		0.230±0.025		0.242±0.014
92°		0.280±0.027		0.247±0.015
94°		0.202±0.028		0.222±0.016
96°		0.234±0.033		0.275±0.020
98°		0.179±0.060		0.175±0.044
80°	790.1	0.329±0.403		
82°		0.196±0.170		
84°		0.222±0.049		
86°		0.247±0.043		
88°		0.134±0.039		
90°		0.198±0.040		
92°		0.118±0.042		
94°		0.221±0.040		
96°		0.202±0.057		
98°		0.065±0.124		

opposite direction to beam depolarization. Work is in progress to correct the $\Delta\sigma_L$ data in Ref. 1, using the more recent knowledge about the beam polarization from Ref. 40. Since this work on the ZGS data is incomplete, the published values have been plotted in Fig. 14.

In addition to beam polarization uncertainties, there is a beam momentum uncertainty of roughly ± 30 MeV/c on the ZGS $\Delta\sigma_L$ data. With the beam uncertainties described above and the quoted target uncertainties for the ZGS results in Ref. 1, as well as with the systematic uncertainties for the LAMPF data, the agreement of the LAMPF and ZGS $\Delta\sigma_L$ values appears quite reasonable.

The discrepancy between the LAMPF and TRIUMF $\Delta\sigma_L$ results is of some concern. Experimenters from both groups⁷⁰ have met to try to understand the source of the discrepancy. From these discussions, various differences

in experimental techniques were noted. Whereas the ZGS and LAMPF target and beam polarizations were essentially purely L -type (longitudinal), the TRIUMF polarizations contained small, but important, transverse components. The orientation of the transmission-counter arrays for the two experiments was opposite (the ZGS orientation was the same as at LAMPF). The orientation of the transmission counters used by LAMPF allowed for monitoring of counter efficiency over most of the counter area, while the TRIUMF orientation allowed for monitoring the efficiency only in the central (beam) region. The TRIUMF orientation was less affected by absorption of low-energy particles, such as deuterons from the $pp \rightarrow \pi d$ reaction, however. There were also differences in the electronic logic, with the LAMPF setup being more elaborate, and with more internal checks. Some of the TRIUMF $\Delta\sigma_L$ data were taken with both signs of the spin-precessing solenoid current, but the LAMPF data with only one sign. Beam anticoincidence counters were used

TABLE X. Fitted values of the coefficients in the expression $C_{LL}(\theta) = \alpha + \beta \cos^2(\theta)$.

T (MeV)	α	β
302.9	0.475±0.007	0.95±0.92
384.6	0.285±0.015	0.36±1.91
434.4	0.197±0.015	-4.55±1.63
485.0	0.131±0.023	3.63±2.50
518.4	0.124±0.008	1.29±0.92
535.4	0.171±0.021	5.43±2.46
569.6	0.165±0.007	2.38±0.81
586.3	0.180±0.013	2.54±1.46
619.8	0.204±0.009	0.59±1.08
636.8	0.205±0.018	1.43±2.20
688.0	0.244±0.010	-1.89±1.32
739.5	0.237±0.006	2.37±0.84
790.1	0.172±0.016	3.25±2.51

TABLE XI. Experimental values of C_{SL} (485 MeV).

$\theta_{c.m.}$	C_{SL}
80°	-0.107±0.157
82°	0.182±0.070
84°	0.089±0.054
86°	0.070±0.050
88°	0.007±0.051
90°	0.022±0.049
92°	0.004±0.052
94°	0.010±0.054
96°	-0.095±0.062
98°	-0.065±0.121

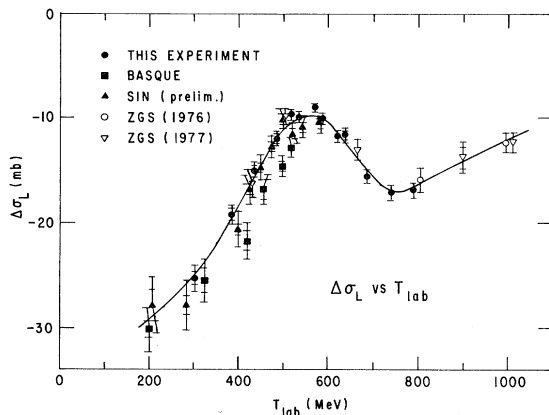


FIG. 14. Measured values of the pp total-cross-section differences $\Delta\sigma_L$ from this experiment, from the ZGS (Ref. 1), from SIN (Ref. 29), and from the BASQUE group at TRIUMF (Ref. 30). The shorter error bars represent the statistical uncertainties only, and the longer ones represent the combined systematic and statistical uncertainties. The curve shown was drawn by eye.

at LAMPF and the ZGS, but not at TRIUMF. This was offset by using beam-defining counters closer to the polarized target at TRIUMF. Finally, the beam polarimeter at TRIUMF was located upstream of the collimator and measured only one spin component, whereas the beam polarimeters at LAMPF were located downstream of the strippers and measured all three spin components.

After the discussions mentioned above, there were several small changes made to the preliminary values of $\Delta\sigma_L$ which had been reported by both groups in the literature.^{27,30} The phase shifts of Arndt *et al.*,⁷¹ have been used to make Coulomb-nuclear corrections to the LAMPF data, instead of the method described by Watanabe,⁷² which had been used earlier. There were also changes made in the quoted systematic uncertainties for the target polarization and the target constant, as described above. The magnitude of the TRIUMF $\Delta\sigma_L$ data from Ref. 30 was normalized downwards 2.6% for the change in target area with temperature and downwards 5.3% for a change to the target polarization. The statistical errors on the TRIUMF results were also increased to account for fluctuations in the data that were larger than expected. A correction to the TRIUMF data was also made which resulted from an error that had been made in the momentum-transfer (t) value ascribed to each transmission counter; the slopes $\partial(\Delta\sigma_L)/\partial t$ of the two sets of data are now in satisfactory agreement. The TRIUMF $\Delta\sigma_{LL}(pp)$ results, with these corrections, are plotted in Fig. 14.

Two cross comparisons of the TRIUMF and LAMPF data give indications of other systematic differences between the two experiments. Corrections due to both effects would tend to move the two sets of $\Delta\sigma_L$ values closer together by a total of $\sim(14\pm 10)\%$, but the uncertainties are large enough in both cases so that no strong conclusion can be reached concerning the magnitude of the remaining discrepancy. The first comparison involves the packing fraction of the polarized targets, which

should be about the same for both targets. This quantity is the average target density divided by the density of the bulk target material, which enters into the calculation of the target constant. The packing fraction is $\sim 64\%$ for the LAMPF $\Delta\sigma_L$ experiment, but it is $8\pm 8\%$ smaller for the TRIUMF $\Delta\sigma_L$ results. Any difference may be caused by different packing procedures, different target volumes and "edge effects," or by different distributions of target-bead sizes, as well as by errors in the measurements of the target density.

The second comparison involves the ratio r of the measured C_{LL} values to the BASQUE phase-shift predictions;¹⁶ this ratio is a measure of the product of beam and target polarizations ($P_B P_T$). Unfortunately, a direct comparison of C_{LL} values between the two experiments is not possible. The TRIUMF target monitor measured a combination of the elastic-scattering spin parameters C_{LL} , C_{LS} , and C_{SS} near $\theta_{c.m.}=70^\circ$, whereas the LAMPF results were for pure C_{LL} near $\theta_{c.m.}=90^\circ$. Hence, a phase-shift analysis is needed to relate the two sets of elastic-scattering data. The following procedure was used: For both experiments, the ratio r was first computed at each energy by averaging over the elastic-scattering acceptance. The value of χ^2 per degree of freedom for the LAMPF C_{LL} data, compared with the BASQUE phase-shift predictions, was found to be close to 1.0 at each energy. The ratio r was then averaged over all energies up to 520 MeV. (In this case, the χ^2 for the average over the energies was poor. The errors on r were increased accordingly. However, no estimate of the error from the phase shifts was included when computing χ^2 .) The final results for r were 1.012 ± 0.029 and 0.958 ± 0.035 for the TRIUMF and LAMPF data, respectively. These results indicate a difference of $(5.6\pm 4.9)\%$ between the LAMPF and TRIUMF C_{LL} or ($P_B P_T$) values. The ratio r from the phase shifts of Arndt *et al.*⁷¹ (solution SF 81) is 0.979 ± 0.030 for the LAMPF data.

We have several criticisms of the TRIUMF results which may or may not be related to the discrepancy. First, we note that there appears to be some source of fluctuations in the individual TRIUMF runs (which are many fewer in number at each energy than the LAMPF runs) that cannot be accounted for. These fluctuations are on the average about two to three times the statistical errors. The existence of these fluctuations, which are not understood, but which may arise from such effects as accidental counts, counter-efficiency changes, and variation of the part of the target sampled by the beam, makes it difficult to argue that they can be accounted for simply by increasing the statistical errors, as was done between the preliminary and final published results. Moreover, at most energies we note that the TRIUMF data were not measured with the full set of possible combinations of solenoid and target-spin directions, so some checks on internal consistency were not available. For the LAMPF results, the χ^2 per degree of freedom of the individual $\Delta\sigma_L$ runs was close to 1.0, as statistically expected. On two or three occasions, when anomalously large fluctuations were encountered in the course of running at LAMPF, it was possible to determine and correct the cause, and those runs were discarded.

Next, we note that whereas all three beam spin components were measured near the polarized target at LAMPF, only one was measured at TRIUMF. Furthermore, this single component was measured upstream of a spin-precessing solenoid and a collimator that reduced the beam intensity by roughly a factor of 1000.^{30,70} At TRIUMF there has been evidence of beam motion with spin orientation from the polarized ion source, and of 5% differences in beam polarization as a function of vertical position within the beam spot at the TRIUMF polarimeter.⁷³ Therefore, it is possible that sizable unknown spin components could have been present in certain parts of the beam spot at the polarimeter (in the *S*- or *L*-type direction), and thus also at the TRIUMF polarized target. Furthermore, because of the observed beam steering caused by the spin-precessing solenoid, the effects of an unmeasured spin component need not cancel when averaging over the solenoid current direction. (We note that problems similar to these are found with the LAMPF beam also. If the LAMPF experiment had used a method of measuring the beam polarization similar to that used at TRIUMF, a systematic error the order of a few percent would have resulted, as described above.)

Finally, we note the results of a comparison of the $\Delta\sigma_L$ values that was made with the phase-shift predictions of Arndt and Roper using the VPI interactive computer program.⁷¹ The phase-shift solution used in this study was the one designated SP82 (spring, 1982). Using the single-energy solution at 500 MeV, which covered laboratory kinetic energies of 450–544 MeV, and removing the three LAMPF $\Delta\sigma_L$ values from this work, led to a drop in χ^2 by 3.1. Removing the ZGS $\Delta\sigma_L$ value at 508 MeV¹ caused an additional drop in χ^2 of 1.0. Naive attempts to fit the TRIUMF $\Delta\sigma_L$ values instead of the LAMPF results using the VPI interactive computer program have not met with success. We conclude from these observations that differences between existing phase-shift solutions can lead to differences of several mb in the predicted values for $\Delta\sigma_L(pp)$. We also conclude that it appears premature to reject any of the $\Delta\sigma_L$ measurements on the basis of phase shifts or dispersion relations^{12,13,15,16,30} at this time.

IV. INTERPRETATION

A. $\Delta\sigma_L$

In terms of the *s*-channel helicity amplitudes of Jacob and Wick⁷⁴ and Goldberger, Grisaru, MacDowell, and Wong,⁷⁵

$$\begin{aligned}\phi_1 &= \langle ++ | ++ \rangle, \\ \phi_2 &= \langle ++ | -- \rangle, \\ \phi_3 &= \langle +- | +- \rangle, \\ \phi_4 &= \langle +- | -+ \rangle, \\ \phi_5 &= \langle ++ | +- \rangle,\end{aligned}\quad (1)$$

the three *pp* total cross sections can be written as⁷⁶

$$\begin{aligned}\sigma_{\text{tot}} &= \frac{1}{2} [\sigma(\rightleftharpoons) + \sigma(\Rightarrow)] = \frac{1}{2} [\sigma(\uparrow\downarrow) + \sigma(\uparrow\uparrow)] \\ &= \frac{2\pi}{k} \text{Im}[\phi_1(0) + \phi_3(0)], \\ \Delta\sigma_L &= \sigma(\rightleftharpoons) - \sigma(\Rightarrow) = \frac{4\pi}{k} \text{Im}[\phi_1(0) - \phi_3(0)],\end{aligned}\quad (2)$$

$$\Delta\sigma_T = \sigma(\uparrow\downarrow) - \sigma(\uparrow\uparrow) = -\frac{4\pi}{k} \text{Im}[\phi_2(0)].$$

In Eqs. (1), + and - refer to the helicities of the protons, and in Eq. (2), *k* is the c.m. momentum, $\sigma(\rightleftharpoons)$ is the total cross section for parallel longitudinal spin states in the laboratory frame, $\sigma(\uparrow\downarrow)$ is the total cross section for antiparallel transverse spin states, etc.

The helicity amplitudes can be decomposed into spin partial waves by the equations^{75,77}

$$\begin{aligned}\phi_1 &= \frac{1}{2ik} \sum d_{00}^J(\theta) \{ (2J+1)R_J + (J+1)R_{J+1,J} + JR_{J-1,J} \\ &\quad + 2[J(J+1)]^{1/2}R^J \}, \\ \phi_2 &= \frac{1}{2ik} \sum d_{00}^J(\theta) \{ -(2J+1)R_J + (J+1)R_{J+1,J} \\ &\quad + JR_{J-1,J} + 2[J(J+1)]^{1/2}R^J \}, \\ \phi_3 &= \frac{1}{2ik} \sum d_{11}^J(\theta) \{ (2J+1)R_{JJ} + JR_{J+1,J} + (J+1)R_{J-1,J} \\ &\quad - 2[J(J+1)]^{1/2}R^J \}, \\ \phi_4 &= \frac{1}{2ik} \sum d_{-11}^J(\theta) \{ -(2J+1)R_{JJ} + JR_{J+1,J} \\ &\quad + (J+1)R_{J-1,J} - 2[J(J+1)]^{1/2}R^J \}, \\ \phi_5 &= \frac{1}{2ik} \sum d_{10}^J(\theta) \{ -[J(J+1)]^{1/2}R_{J+1,J} \\ &\quad + [(J+1)]^{1/2}R_{J-1,J} + R^J \}.\end{aligned}\quad (3)$$

The $d_{ij}^J(\theta)$ are the reduced spherical harmonics.⁷⁸ At $\theta_{\text{c.m.}}=0^\circ$,

$$d_{00}^J(0) = 1 = d_{11}^J(0),$$

$$d_{-11}^J(0) = 0 = d_{10}^J(0).$$

Therefore, $\phi_4(0) = 0 = \phi_5(0)$; physically, this is a consequence of helicity conservation at 0° . The spin-singlet partial waves ($^1S_0, ^1D_2, ^1G_4, \dots$) in these equations have $J=L=\text{even}$, and the uncoupled triplet partial waves ($^3P_1, ^3F_3, ^3H_5, \dots$) have $J=L=\text{odd}$. These waves correspond to

$$R_J = \cos(\rho_J) \exp(2i\delta_J) - 1, \quad (4)$$

$$R_{JJ} = \cos(\rho_{JJ}) \exp(2i\delta_{JJ}) - 1,$$

respectively, where ρ_J and ρ_{JJ} are the inelasticities and δ_J and δ_{JJ} are the phase shifts. The coupled triplet partial waves ($^3P_2, ^3F_2, ^3F_4, ^3H_4, \dots$), with $J=L \mp 1 = \text{even}$, corre-

spend to

$$R_{J\pm 1,J} = \cos(\rho_{\pm J}) \cos(2\epsilon_J) \exp(2i\delta_{\pm J}) - 1, \quad (5)$$

$$R^J = i \sin(2\epsilon_J) \exp[i(\delta_{+J} + \delta_{-J} + \alpha_J)].$$

If the amplitudes ϕ_s , ϕ_t , and ϕ_T are defined as

$$\begin{aligned} \phi_s &= (\phi_1 - \phi_2)/2 = \frac{1}{2ik} \sum d_{00}^J(\theta) (2J+1) R_J, \\ \phi_t &= (\phi_1 + \phi_2)/2 \\ &= \frac{1}{2ik} \sum d_{00}^J(\theta) \{ (J+1) R_{J+1,J} + J R_{J-1,J} \\ &\quad + 2[J(J+1)]^{1/2} R^J \}, \end{aligned} \quad (6)$$

$$\phi_T = \phi_3,$$

then the contributions of the spin-singlet and spin-triplet partial waves to the total cross section can be separated as follows:^{12,14,17,79}

$$\begin{aligned} \sigma^s &= \frac{2\pi}{k} \text{Im}\phi_s(0^\circ) = \frac{1}{8} (2\sigma_{\text{tot}} + 2\Delta\sigma_T + \Delta\sigma_L), \\ \sigma^t &= \frac{2\pi}{k} \text{Im}\phi_t(0^\circ) = \frac{1}{8} (2\sigma_{\text{tot}} - 2\Delta\sigma_T + \Delta\sigma_L), \\ \sigma^T &= \frac{2\pi}{k} \text{Im}\phi_T(0^\circ) = \frac{1}{4} (2\sigma_{\text{tot}} - \Delta\sigma_L). \end{aligned} \quad (7)$$

The quantity σ^s contains only spin-singlet terms, σ^t contains only coupled-spin-triplet terms, and σ^T contains only spin-triplet terms (with 3P_0 only in σ^t). The sum $\sigma^s + \sigma^t + \sigma^T$ gives the total cross section σ_{tot} . Note that the quantity $\sigma^T = \sigma(\Rightarrow)/2$ and the quantity

$$\sigma^f = [2\sigma(\uparrow\uparrow) - \sigma(\Rightarrow)]/4$$

both consist of parallel spin terms. These require $S=1$ or spin-triplet contributions only.

Figures 14, 15, and 16 show the measured total cross sections $\Delta\sigma_L$ from Refs. 1, 29, 95, and from this experiment, σ_{tot} from Refs. 80–93, and $\Delta\sigma_T$ from Refs. 31 and 94–96. Three values of $\Delta\sigma_T$ were measured by this group in a separate experiment as a check.³¹ They seem to agree well with the preliminary Saclay values,⁹⁶ but fall below the TRIUMF values,⁹⁵ as mentioned above, and

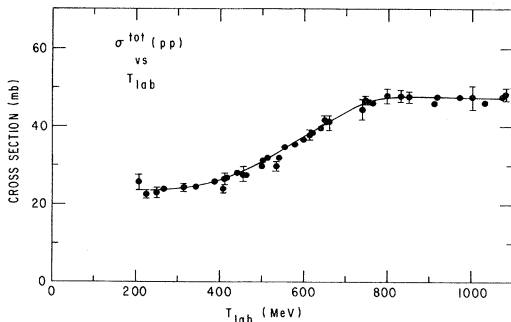


FIG. 15. Measured values of pp total cross sections vs laboratory beam energy, from Refs. 80–93. The errors shown represent the combined systematic and statistical uncertainties. The curve was drawn by eye.

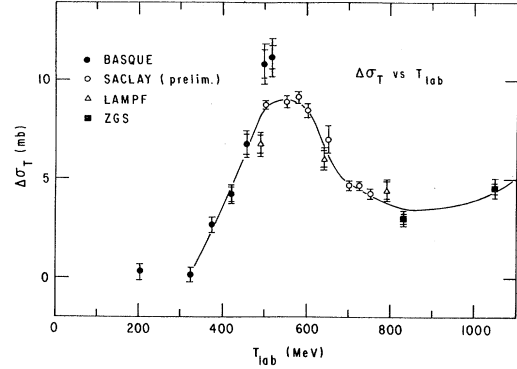


FIG. 16. Measured values of pp total-cross-section differences $\Delta\sigma_T$, from the BASQUE group at TRIUMF (Ref. 95), Saclay (Ref. 96), LAMPF (Ref. 31) and the ZGS (Ref. 94). The shorter error bars represent the statistical uncertainties only, and the longer ones represent the combined systematic and statistical uncertainties. The curve shown was drawn by eye.

somewhat above the older ZGS data.⁹⁴

The curves drawn by eye through the three pp total cross sections in Figs. 14–16 were used to compute the quantities σ^s , σ^t , and σ^T . These are given in Figs. 17–19, respectively, along with representative errors. These correspond to the quoted measurement uncertainties (combined statistical and systematic errors) and an estimated uncertainty in drawing the smooth curve through the data.

Structure is apparent in all three cross sections in Figs. 17–19. To assist in understanding the source of this structure, the cross sections are shown decomposed into individual partial waves in these same figures, using the Arndt *et al.* phase shifts.⁷¹ Some of the higher partial waves, which give small contributions, are omitted for clarity. As can be seen from Fig. 17, the shoulder in σ^s near 600 MeV is partially caused by the resonancelike behavior of the 1D_2 partial wave. Near this energy, the only other major contribution comes from the 1S_0 partial wave, which exhibits a smoother behavior with energy than the 1D_2 partial wave. The main contributions to σ^t (Fig. 18) are from 3P_0 and the coupled triplet waves 3P_2 and 3F_2 . According to Arndt's phase shifts, the 3P_0 partial wave exhibits a relatively broad maximum in the ener-

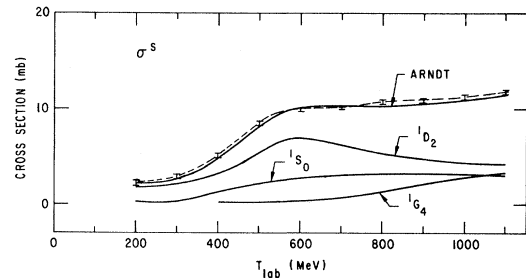
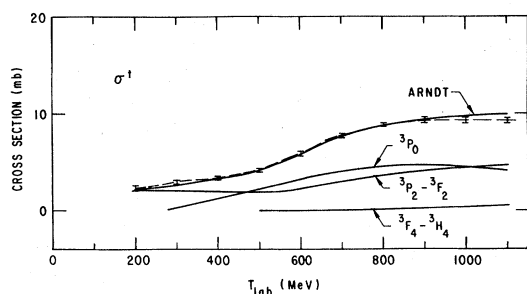
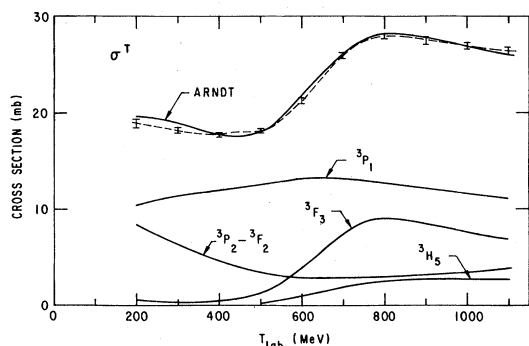
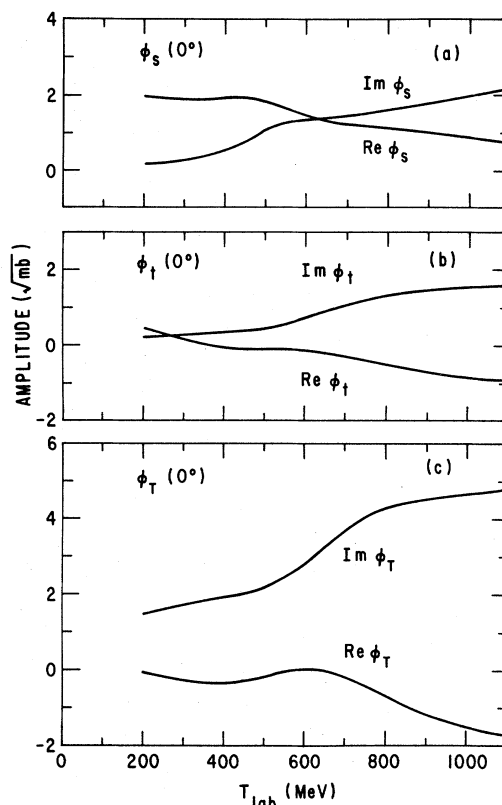


FIG. 17. Curve of the quantity σ^s constructed from the curves shown in Figs. 14–16, with representative error bars. Also shown is the Arndt *et al.* phase-shift prediction (Ref. 71), together with the contributions of various partial waves.

FIG. 18. Same as Fig. 17, but for the quantity σ^t .

gy range near 800 MeV. Finally, in Fig. 19, the peak in σ^T near 800 MeV is seen to be related to the resonancelike behavior of the 3F_3 partial wave. The uncoupled triplet wave 3P_1 exhibits a broad maximum and the coupled triplet waves (3P_2 - 3F_2) a broad minimum. These latter three waves dominate σ^T at lower energies.

Grein and Kroll¹³ have performed dispersion-relation calculations to obtain the real parts of the three forward amplitudes from the three total cross sections σ_{tot} , $\Delta\sigma_L$, and $\Delta\sigma_T$. These real parts have been used as inputs to the phase-shift analyses of Arndt *et al.* and Hoshizaki. The behavior of the amplitudes corresponding to σ^s , σ^t , and σ^T is shown in Fig. 20. A clear resonancelike behavior is observed for ϕ_T (see also Ref. 12), which is presumably from the 3F_3 partial wave. Weaker structure is also observed in ϕ_s and ϕ_t , which is presumably from the 1D_2 and 3P_0 , 3P_2 , or 3F_2 waves, respectively. These calculations by Grein and Kroll have been criticized by Dubois *et al.*⁹⁷ as being incompatible with phase-shift results below pion production threshold. On the other hand, Grein and Kroll are unable to reproduce the dispersion-relation results of Dubois *et al.*, and have criticized the imaginary parts of their amplitudes derived from the three *pp* total cross sections. The real parts of the amplitudes obtained by Grein and Kroll also differ somewhat from various phase-shift predictions, but the differences are comparable to the differences *between* various phase-shift solutions. A more accurate determination of the real parts of the amplitudes awaits measurements of various spin param-

FIG. 19. Same as Fig. 17, but for the quantity σ^T .FIG. 20. The amplitudes corresponding to σ^s , σ^t , and σ^T , as found from the dispersion-relation calculations of Grein and Kroll (Ref. 13).

ters in the Coulomb-nuclear interference region.

The three total cross sections can be decomposed into a sum of elastic and inelastic contributions. The elastic contributions are

$$\begin{aligned} \sigma^{el} &= \int (d\sigma/d\Omega)_{el} d\Omega, \\ \Delta\sigma_T(\text{elastic}) &= - \int (C_{NN} + C_{SS})(d\sigma/d\Omega)_{el} d\Omega, \quad (8) \\ \Delta\sigma_L(\text{elastic}) &= -2 \int C_{LL}(d\sigma/d\Omega)_{el} d\Omega. \end{aligned}$$

From C_{LL} data over a wide angular range from a ZGS experiment and C_{LL} data near 90° c.m. from this experiment and others, it is possible to derive $\Delta\sigma_L(\text{elastic})$.⁹⁸ Results from a SIN experiment,⁹⁹ as well as those from the ZGS, are shown in Fig. 21. The spin-averaged elastic cross-section values are also shown (Refs. 81–83, 85, 90, 92, 93, and 100–108). Below 600 MeV, values of $\Delta\sigma_T(\text{elastic})$ have also been obtained by a group at SIN,⁹⁹ but the only data available at higher energies at this time are at 6 GeV/c.

The inelastic contribution to $\Delta\sigma_L$ can be found by taking the difference

$$\Delta\sigma_L(\text{inelastic}) = \Delta\sigma_L - \Delta\sigma_L(\text{elastic});$$

the results are shown in Fig. 22. A similar procedure can be followed to determine the elastic and inelastic cross sections corresponding to σ^T :

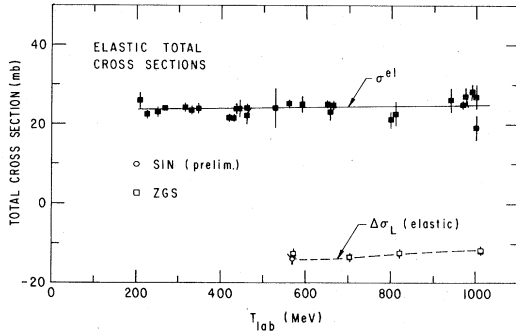


FIG. 21. Measured values of the total elastic cross section and the total-elastic-cross-section difference $\Delta\sigma_L$, from the sources given in the text.

$$\sigma^T(\text{elastic}) = \frac{1}{4} [2\sigma^{\text{el}} - \Delta\sigma_L(\text{elastic})],$$

$$\sigma^T(\text{inelastic}) = \sigma^T - \sigma^T(\text{elastic}).$$

These are also shown in Fig. 22. The results of Arndt's phase-shift analysis⁷¹ are presented for comparison.

In the past, it has sometimes been asserted that the structure in $\Delta\sigma_L$ near 800 MeV was largely caused by the variation with energy of $\Delta\sigma_L(\text{elastic})$.^{14,109} However, it can be seen in Fig. 22 that the structure in $\Delta\sigma_L$ (and peak in σ^T) arises largely from the structure in the inelastic contribution, as expected from a highly inelastic dibaryon. This behavior is contrary to current models of pion pro-

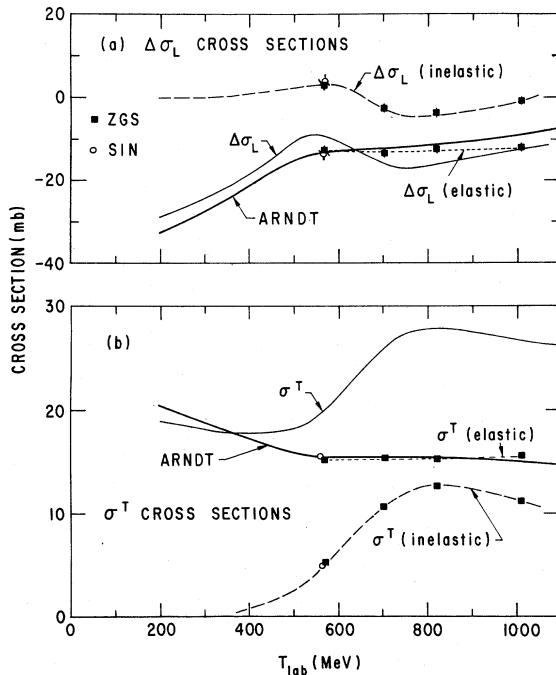


FIG. 22. Measured values of the total elastic and inelastic cross sections (a) for the cross-section difference $\Delta\sigma_L$, and (b) for the cross section σ^T , found as described in the text. The Arndt *et al.* phase-shift predictions (Ref. 71) are also shown.

duction which omit dibaryons (see Ref. 98).

The treatment of the total-cross-section results here is similar to the work of Bystricky, Lehar, and Winternitz^{110,111} based on the Saclay phase shifts. These phase shifts had predicted structure in $\Delta\sigma_L$ qualitatively similar to the experimental data *before* any $\Delta\sigma_L$ measurements had been made at the ZGS. In a recent paper, Bystricky *et al.*¹⁴ discuss the behavior of the total cross sections in terms of their most recent phase shifts. The experimental values of σ^s , σ^t , and σ^T obtained here are reasonably well reproduced by the Saclay phase shifts. However, the detailed behavior of $\Delta\sigma_L(\text{elastic})$ is somewhat different from the Saclay predictions because the new ZGS C_{LL} results⁹⁸ were not included in their data base. It is possible that some of the conclusions concerning dibaryons reached by Bystricky *et al.* may be changed as a consequence of the new experimental values of $\Delta\sigma_L(\text{elastic})$.

B. $\Delta\sigma_L$ slope

The experimental values of the slope S_L of $\Delta\sigma_L$ with the four-momentum transfer-squared t shown in Fig. 9 can be compared with predictions derived from other data. The expected value of S_L is given by

$$S_L \equiv \frac{\partial(\Delta\sigma_L)}{\partial t} = -2C_{LL}(pp \rightarrow pp) \left[\frac{d\sigma}{dt} \right]_{\text{el}} - 2C_{LL}(pp \rightarrow \pi d) \left[\frac{d\sigma}{dt} \right]_{\pi d} \frac{dt_{\pi d}}{dt_{\text{el}}} - 2C_{LL}(pp \rightarrow NN\pi) \left[\frac{d\sigma}{dt} \right]_{NN\pi} \frac{dt_{NN\pi}}{dt_{\text{el}}} - \dots \quad (9)$$

For this comparison, values of $\Delta\sigma_L(t_i)$ are used which are *not* corrected for Coulomb-nuclear interference effects. This has the advantage that different Coulomb-nuclear corrections do not need to be applied for different phase-shift solutions. Thus, new phase-shift solutions can be directly compared to the experimental results presented here. Furthermore, the evaluation of inelastic contributions becomes more complicated if Coulomb-corrected slopes are used.

In Eq. (9) above, detection efficiencies for the different contributions to S_L should also be included. For example, particles may have been scattered or absorbed in the polarized target or transmission counters, depending on their energy and particle type. Such effects are small for elastic scattering near $\theta_{\text{c.m.}} = 0^\circ$, but can be important for some of the inelastic reactions.

The elastic contribution to the slope was estimated from Arndt's phase shifts.⁷¹ The value of $2C_{LL}(d\sigma/dt)$ was calculated for elastic scattering as a function of t . The average value over the range of t in these measurements was estimated, giving somewhat more weight to the slope at larger angles, where $2C_{LL}(d\sigma/dt)$ varies more slowly. From the variation of S_L with t , and from a comparison of the phase-shift predictions of Arndt *et al.*⁷¹ and Bugg *et al.*,¹¹² it was estimated that this prediction of

the elastic contribution to the slope has an uncertainty of about

$$\pm 5-10 \text{ mb}/(\text{GeV}/c)^2 .$$

The effect of multiple scattering of the protons in the polarized target is smaller than

$$5 \text{ mb}/(\text{GeV}/c)^2 ,$$

except for the very smallest counters. This estimate of the elastic contribution to S_L is shown in Fig. 9. It can be seen that the agreement with the experimental results is good near 300 MeV and between 700 and 800 MeV. The agreement near 300 MeV is encouraging, since the inelastic cross section and contribution to S_L are essentially zero at that energy.

As mentioned above, the transmitted beam and elastically scattered protons were not the only particles detected by the transmission counters. Inelastic events could also have been detected and could have affected the observed slope. For the $pp \rightarrow \pi d$ reaction, for example, the deuteron laboratory angle is kinematically limited to less than 15° at LAMPF energies. Furthermore, the cross section for the reaction peaks near 600 MeV. At higher energies, the cross section drops and the maximum deuteron angle increases, causing a decrease in the number of deuterons detected by the transmission counters. At lower energies, all inelastic cross sections decrease, reducing the effect on the slope S_L as well.

The contribution of the $pp \rightarrow \pi d$ reaction to the slope was estimated as follows. The compiled data in Ref. 61 were used to obtain the cross section as a function of $\theta_{c.m.}$. Then $\theta_{c.m.}$ was converted to θ_{lab} , and finally to the equivalent t for pp elastic scattering. The value of $C_{LL}(pp \rightarrow \pi d)$ was taken to be constant over the angular range of the transmission counters, using values from the preliminary SIN results.¹¹³ The $pp \rightarrow \pi d$ contribution to Eq. (9) consisted of two parts: (a) fast forward deuterons corresponding to $\theta_{\pi,lab} \sim 180^\circ$, and (b) slow forward deuterons corresponding to $\theta_{\pi,lab} \sim 0^\circ$. (The contribution from forward pions is included in the case of slow forward deuterons.) No corrections were made for absorption or interactions of the deuterons in the polarized target or transmission counters. Even though the slow forward deuterons at the lower beam energies would have been stopped before passing completely through the target and counters, the contribution of these deuterons to S_L was only about 25–35% of the full $pp \rightarrow \pi d$ contribution. Furthermore, the slow forward deuterons were accompanied by forward pions, which were not stopped.

The results of the $pp \rightarrow \pi d$ estimate, added to the elastic-scattering contribution, are also shown in Fig. 9. The uncertainty on the prediction of S_L from both pp elastic and $pp \rightarrow \pi d$ reactions is roughly $\pm 20 \text{ mb}/(\text{GeV}/c)^2$. Calculations of the $pp \rightarrow \pi d$ contribution could not be performed at other energies for lack of $C_{LL}(pp \rightarrow \pi d)$ data. However, a limit to the magnitude of the slope was obtained from the cross section, assuming $|C_{LL}| = 1$; it was found to be less than $20 \text{ mb}/(\text{GeV}/c)^2$ at both 300 and 800 MeV. Therefore, the agreement between the calculated and observed slopes is considerably improved by the addition of the $pp \rightarrow \pi d$ reaction.

A calculation of the effect of the $pp \rightarrow NN\pi$ reaction on the observed slope S_L is very complicated, requiring knowledge of C_{LL} for the reaction as well as the cross section. The existing data are too meager to perform such a calculation. However, an attempt was made to test whether the difference between the observed and calculated slopes from $pp \rightarrow \pi d$ and pp elastic reactions was consistent with $pp \rightarrow NN\pi$ reactions. The laboratory angular distribution of protons from $pp \rightarrow pN\pi$ was calculated, assuming pure phase-space distribution for the three outgoing particles. It was found that the difference in Fig. 9 could be explained with values of $C_{LL}(pp \rightarrow pN\pi)$ that are large and negative in the forward direction. The only existing results^{114,115} are consistent with this requirement near 500 MeV, but are small and positive at 800 MeV.

In conclusion, we find that the observed slope of $\Delta\sigma_L$ with t is consistent with existing cross-section and C_{LL} data on $pp \rightarrow pp, \pi d, NN\pi$ in the energy range of this experiment. At the lowest energy, there is agreement with the slope expected from elastic scattering alone. In addition, it is suggested that C_{LL} for $pp \rightarrow NN\pi$ should be generally large and negative between about 450 and 600 MeV.

C. C_{LL}

At $\theta_{c.m.} = 90^\circ$ there are three independent amplitudes for pp elastic scattering.¹¹⁶ In terms of the s -channel helicity amplitudes introduced above, the following relations hold at 90° c.m.:

$$\phi_4 = -\phi_3 ,$$

$$\phi_5 = 0 .$$

In terms of the three amplitudes ϕ_s , ϕ_t , and ϕ_T ,

$$\phi_s = (\phi_1 - \phi_2)/2 ,$$

$$\phi_t = (\phi_1 + \phi_2)/2 , \quad (10)$$

$$\phi_T = \phi_3 ,$$

the following expressions are valid for pp elastic scattering at 90° c.m.:

$$d\sigma/d\Omega = |\phi_s|^2 + |\phi_t|^2 + |\phi_T|^2 ,$$

$$C_{NN}(d\sigma/d\Omega) = -|\phi_s|^2 + |\phi_t|^2 + |\phi_T|^2 \\ = (N, N; 0, 0)(d\sigma/d\Omega) , \quad (11)$$

$$C_{LL}(d\sigma/d\Omega) = -|\phi_s|^2 - |\phi_t|^2 + |\phi_T|^2 \\ = (L, L; 0, 0)(d\sigma/d\Omega) ,$$

$$C_{SS}(d\sigma/d\Omega) = -|\phi_s|^2 + |\phi_t|^2 - |\phi_T|^2 \\ = (S, S; 0, 0)(d\sigma/d\Omega) .$$

From these relations at 90° c.m.,

$$C_{NN} - C_{LL} - C_{SS} = 1$$

and, consequently,

$$C_{NN} \geq C_{LL} ,$$

$$C_{NN} \geq C_{SS} , \quad (12)$$

$$-C_{LL} \geq C_{SS} .$$

Also, the magnitude of the three independent amplitudes at 90° can be obtained from $d\sigma/d\Omega$, C_{NN} , and C_{LL} (Refs. 28,79, and 117–120) as follows:

$$\begin{aligned} |\phi_s|^2 &= (d\sigma/d\Omega)(1 - C_{NN})/2, \\ |\phi_t|^2 &= (d\sigma/d\Omega)(C_{NN} - C_{LL})/2, \\ |\phi_T|^2 &= (d\sigma/d\Omega)(1 + C_{LL})/2. \end{aligned} \quad (13)$$

Again, note that at any angle, the amplitude ϕ_s contains contributions from spin-singlet partial waves only, ϕ_t from coupled-spin-triplet partial waves only, and ϕ_T from spin-triplet waves only [see Eqs. (3) and (6)].

It is possible to find values of these amplitudes at 90° and their relative phases from existing data. Experimental values of $d\sigma/d\Omega$,^{101,103,121–136} C_{NN} ,^{137–153} and C_{LL} from this experiment and Refs. 26, 137, 139, 144, 154, 155 are given in Figs. 23–25. The curves shown were drawn by eye. The data are shown with combined systematic and statistical uncertainties. Values of C_{LL} were obtained from C_{KP} data^{137,139} using the relations¹⁵⁶

$$\begin{aligned} C_{NN} - C_{LL} - C_{SS} &= 1, \\ C_{LL} &= C_{KP} + (C_{NN} - 1)/2, \end{aligned}$$

which are valid at 90° . There is generally good agreement among all data, with few exceptions. The large uncertainties in the values of C_{NN} near 700 MeV are caused in part because C_{NN} is large, so that systematic uncertainties in beam and target polarization normalizations become significant compared to statistical uncertainties. Conversely, the total uncertainties on C_{LL} are generally smaller than on C_{NN} because C_{LL} is smaller in magnitude. The inequality in Eq. (12) can be seen to be verified by the data in Figs. 24 and 25.

The experimental magnitudes of the 90° c.m. amplitudes shown in Fig. 26 were estimated from the curves in Figs. 23–25. Estimates of the uncertainties in $d\sigma/d\Omega$ and C_{NN} dominate the errors shown for the amplitudes; the contribution from C_{LL} is usually small. Note that the magnitudes of the amplitudes at 90° c.m. are comparable

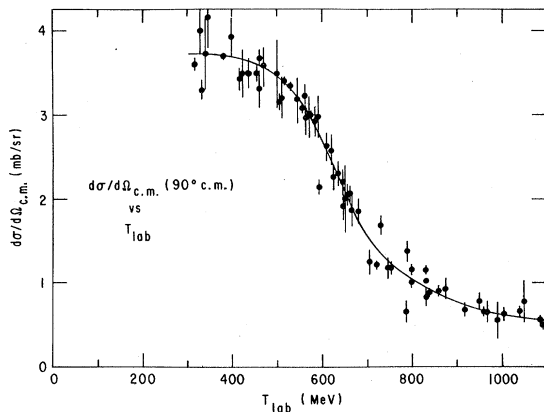


FIG. 23. Measured values of $d\sigma/d\Omega(90^\circ)$, from the sources given in the text. The errors shown represent the combined systematic and statistical uncertainties. The curve was drawn by eye.

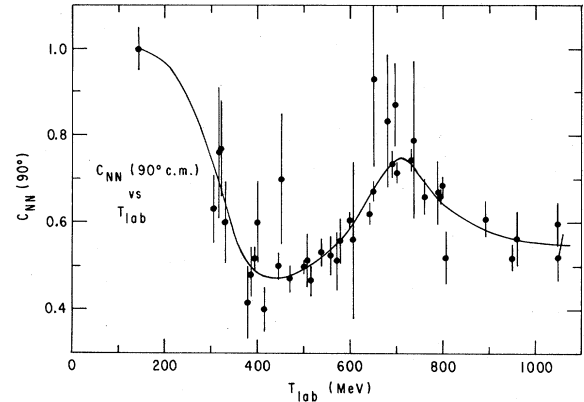


FIG. 24. Measured values of $C_{NN}(90^\circ)$, from the sources given in the text. The errors shown represent the combined systematic and statistical uncertainties. The curve was drawn by eye.

to those at 0° at low energies, but fall far below the forward amplitudes at higher energies (see Fig. 19).

Also shown in Fig. 26 are the predictions of the phase shifts of Arndt *et al.*,⁷¹ which exhibit resonancelike behavior in both the 1D_2 and 3F_3 partial waves. The agreement is quite good over the full energy range. This is expected, since most of the data have been incorporated into the data base used to determine the phase shifts. The magnitudes of all three amplitudes are somewhat larger than the phase-shift predictions between 500 and 600 MeV because of the recent high-precision values of $d\sigma/d\Omega$ by Chatelain *et al.*,¹³⁵ which were not in the Arndt *et al.* phase-shift data base. The structure in $|\phi_s|$ near 700 MeV originates from the peak in C_{NN} ; the phase-shift solution smooths this peak.

The magnitudes of the amplitudes all exhibit some structure as a function of energy. However, in general, many partial waves contribute to each amplitude, making the interpretation difficult. For example, the 1D_2 partial wave contributes only to ϕ_s , and the resonancelike

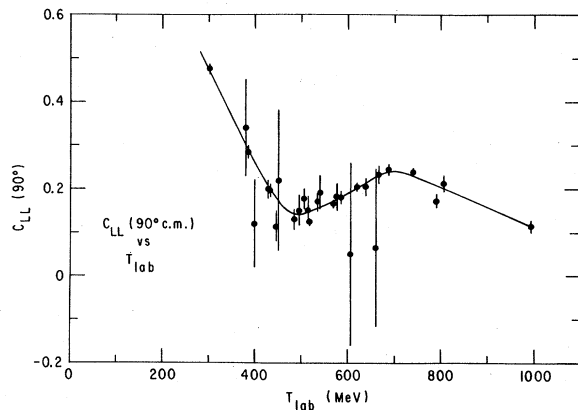


FIG. 25. Measured values of $C_{LL}(90^\circ)$, from the sources given in the text. The errors shown represent the combined systematic and statistical uncertainties. The curve was drawn by eye.

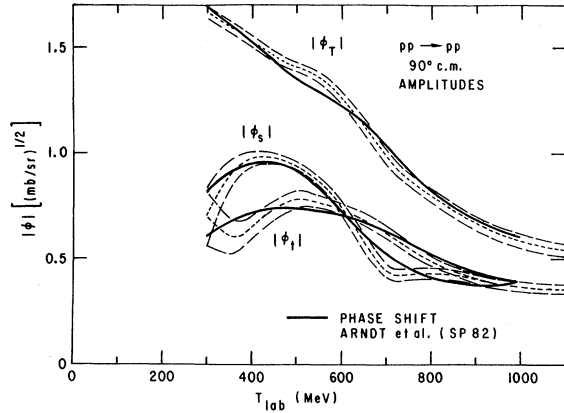


FIG. 26. Magnitudes of the amplitudes ϕ_s , ϕ_t , and ϕ_T , as found from the curves in Figs. 23–25. The central values are indicated by the short-dashed curve, and the range of values is indicated by the long-dashed curves. Also shown are the Arndt *et al.* phase-shift predictions (Ref. 71).

behavior of the 1D_2 partial wave occurs at an energy where $|\phi_s|$ is rapidly decreasing with energy. A similar event holds for the 3F_3 partial wave (which contributes only to ϕ_T). No peaks are apparent near the expected energies. We observe that the structure exhibited by ϕ_t , which contains neither 1D_2 nor 3F_3 partial waves, is similar to that of ϕ_s and ϕ_T . At those energies, it is expected that the principal contribution to ϕ_t would be the 3P_0 , 3P_2 , and 3F_2 partial waves, so that one of these may be responsible for this structure.²⁸ We note that the phase-shift analysis of Dzhgarkava, Kazarnov, Strakhota, and Khayatov¹⁵⁷ at 590 MeV claimed evidence for a 3P_0 resonance.

The relative phases between the amplitudes ϕ_s , ϕ_t , and ϕ_T can be obtained from measurements of other *pp* elastic-scattering parameters at 90° c.m., such as

$$D_{NN}(d\sigma/d\Omega) = 2 \operatorname{Re}(\phi_t \phi_T^*) = (N, 0; N, 0)(d\sigma/d\Omega) \\ = D(d\sigma/d\Omega),$$

$$D_{SS}(d\sigma/d\Omega) = 2 \operatorname{Re}(\phi_s \phi_T^*) \cos\theta_{\text{lab}} \\ = (S, 0; S, 0)(d\sigma/d\Omega) = R(d\sigma/d\Omega), \quad (14)$$

$$D_{LS}(d\sigma/d\Omega) = 2 \operatorname{Re}(\phi_s \phi_t^*) \sin\theta_{\text{lab}} \\ = (L, 0; S, 0)(d\sigma/d\Omega) = A(d\sigma/d\Omega),$$

where θ_{lab} is the laboratory angle corresponding to $\theta_{\text{c.m.}} = 90^\circ$. The overall phase cannot be obtained experimentally, but is available from phase-shift analyses. Furthermore, a change in the sign of all the absolute phases β_s , β_t , and β_T of the amplitudes ϕ_s , ϕ_t , and ϕ_T is seen to leave the values of D_{NN} , D_{SS} , and D_{LS} unchanged from Eq. (14) above.

The experimental data for D_{NN} (Refs. 126 and 158–167), D_{SS} (Refs. 117, 126, 160, 165, 166, 168, and 169), and D_{LS} (Refs. 117, 160, 165, 166, and 169) are shown in Figs. 27–29. It is clear that the number of measurements is smaller and the precision of the results is generally poorer than for $d\sigma/d\Omega$, C_{NN} , and C_{LL} . A

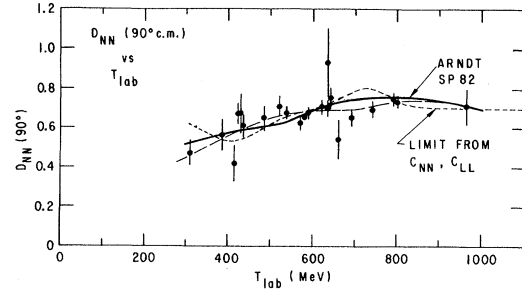


FIG. 27. Measured values of $D_{NN}(90^\circ)$, from the sources given in the text. The errors shown represent the combined systematic and statistical uncertainties. Also shown are a curve drawn by eye, the Arndt *et al.* phase-shift prediction (Ref. 71), and the limit on this quantity found from $C_{NN}(90^\circ)$ and $C_{LL}(90^\circ)$.

smooth curve drawn by eye through the experimental data, and the phase-shift predictions of Arndt *et al.*⁷¹ are also shown.

On the basis of Eq. (14) and the triangle inequality, constraints on the spin observables at 90° c.m. can be found. For example,

$$|D_{NN}(d\sigma/d\Omega)| = |2 \operatorname{Re}\phi_t \phi_T^*| \leq 2 |\phi_t| |\phi_T|.$$

Then, from Eq. (13),

$$|D_{NN}| \leq [(1 + C_{LL})(C_{NN} - C_{LL})]^{1/2}, \\ |D_{SS}/\cos\theta_{\text{lab}}| \leq [(1 - C_{NN})(1 + C_{LL})]^{1/2}, \quad (15) \\ |D_{LS}/\sin\theta_{\text{lab}}| \leq [(1 - C_{NN})(C_{NN} - C_{LL})]^{1/2}.$$

These limits are shown as dashed curves in Figs. 27–29. It can be seen that in some cases the experimental values exceed these limits, but usually by no more than two standard deviations. In general, the data are close to the limits, indicating that ϕ_s , ϕ_t , and ϕ_T are roughly parallel. Finally, it should be noted that the structure in the limits for D_{NN} and D_{SS} near 700 MeV are a consequence of the peak in C_{NN} .

The amplitudes ϕ_s , ϕ_t , ϕ_T were determined from $d\sigma/d\Omega$, C_{NN} , C_{LL} , D_{NN} , $D_{SS}/\cos\theta_{\text{lab}}$, and $D_{LS}/\sin\theta_{\text{lab}}$ using a Monte Carlo procedure. The curves drawn by eye through the experimental data in Figs. 23–25 and 27–29 were used to obtain the values of these six quantities. The uncertainties were calculated from the quoted total errors on the experimental results and from the spread in the

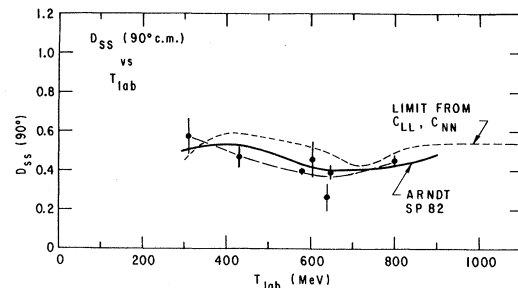


FIG. 28. Same as Fig. 27, but for $D_{SS}(90^\circ)$.

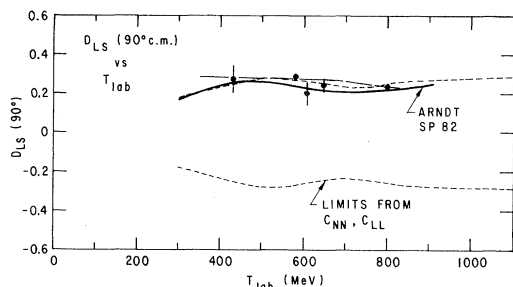


FIG. 29. Same as Fig. 28, but for $D_{LS}(90^\circ)$.

data. The values and uncertainties estimated from the Monte Carlo program for the magnitudes of the amplitudes agreed with the values in Fig. 26.

The relative phases $(\beta_s - \beta_t)$ and $(\beta_T - \beta_t)$ and the errors from the Monte Carlo program are shown in Fig. 30. The phase-shift predictions of Arndt *et al.*⁷¹ are again shown for comparison. It can be seen that the relative phases are indeed nearly the same, and strong energy dependence is not observed. The presence of resonance-like behavior in the 1D_2 and 3F_3 partial waves, which affect $(\beta_s - \beta_t)$ and $(\beta_T - \beta_t)$, respectively, is apparently masked by the large number of partial waves contributing to the 90° c.m. amplitudes.

The two low values of $(\beta_s - \beta_t)$ near 700 MeV arise from the peak in C_{NN} and appear to be anomalous. If the C_{NN} peak were chosen to be less pronounced in Fig. 24, the low $(\beta_s - \beta_t)$ values would increase to be more in line with the other points and with the phase-shift predictions. However, as mentioned earlier, there is a discrete ambiguity of the amplitudes corresponding to a simultaneous change in sign of β_s , β_t , and β_T . The sign of the results plotted in Fig. 30 was chosen to agree best with the phase-shift predictions. A sign change for the 800- and 850-MeV data would lead to a smoother energy variation without the need to modify $C_{NN}(90^\circ \text{ c.m.})$ near 700 MeV or to modify the low values of $(\beta_s - \beta_t)$ near that energy.

Finally, we note that it is our opinion that this choice of amplitudes at 90° c.m. is most useful for analyses in the

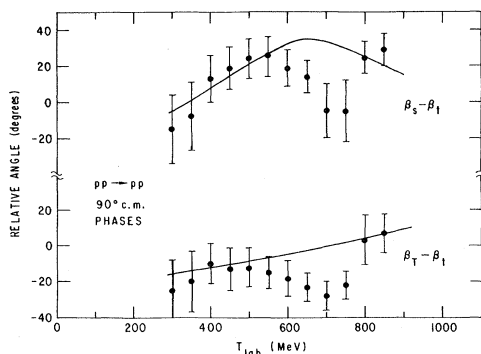


FIG. 30. Values of the relative phases $(\beta_s - \beta_t)$ and $(\beta_T - \beta_t)$, found as described in the text. The curves shown are predictions of the Arndt *et al.* phase shifts (Ref. 71).

foreseeable future. Essentially these same amplitudes were used by Kumekin, Meshcheryakov, Nurushev, and Stoletov¹¹⁷ in their early amplitude analysis near 600 MeV, as well as by Svarc, Bajzer, and Furic.¹¹⁹ The use of this formalism permits the determination of the magnitudes of these amplitudes at higher energies, where C_{NN} , C_{LL} , and $d\sigma/d\Omega$ data already exist. The rapidly falling cross section for pp elastic scattering at 90° makes all spin measurements more difficult with increasing energy, however. Moreover, quantities such as D_{NN} , D_{SS} , and D_{LS} will become even more difficult to measure above ~ 1000 MeV because the analyzing power of polarimeters used to measure the spin of the outgoing particles decreases with energy. Spin parameters such as C_{NN} and C_{LL} , however, which use polarized targets, do not have the latter problem.

V. SUMMARY

We have carried out a series of measurements of $\Delta\sigma_L$, the difference in the total cross sections for pure longitudinal parallel and antiparallel spin states, in proton-proton scattering. At the same time we also measured the spin correlation parameter C_{LL} for pp elastic scattering for center-of-mass angles between 80° and 98° . Results on the slope $\partial(\Delta\sigma_L)/\partial t$ with the four-momentum transfer squared t were also found. Data were taken at 13 laboratory energies between 300 and 800 MeV. The principal aim of this work was to check the previous results on $\Delta\sigma_L$ from ZGS measurements, which had been questioned, and to search for new structure. For this purpose, many systematic checks of the data were made, and new methods of data analysis were used. The resulting statistical errors on $\Delta\sigma_L$ are generally ≤ 0.5 mb, and the overall normalization uncertainty is estimated to be 4.1%. The errors on the slope are generally ≤ 15 mb/(GeV/c)², and errors on C_{LL} at 90° c.m. are estimated to be ≤ 0.02 .

The $\Delta\sigma_L$ results are generally in good agreement with previous data measured at the ZGS and at SIN, but are in sizable disagreement with recent results from TRIUMF. Attempts have been made to understand the sources of this discrepancy, which have involved extensive studies and discussions between experimenters from both groups. These resulted in a modification of the preliminary results which had been reported by each group, but the discrepancy still remains. Possible sources of the disagreement involve details of the differences in the experimental techniques and procedures used by the two groups. We note that more studies of systematic effects and checks of internal consistency were generally carried out at LAMPF than at TRIUMF, however. No new structure was found in the data.

With the use of other total-cross-section data, the $\Delta\sigma_L$ results were used to obtain curves of the quantities σ^s , which contains only spin-singlet terms, σ^t , which contains only coupled-spin-triplet terms, and σ^T , which contains only spin-triplet terms. All three of these were found to contain structure. The partial-wave analysis of Arndt *et al.* suggests that the structure in σ^s is due to the resonantlike behavior in the 1D_2 partial wave, and that in σ^T to the 3F_3 partial wave. That in σ^t is probably due to

the 3P_0 partial wave or the $({}^3P_2, {}^3F_2)$ partial-wave pair. With the use of additional data, $\Delta\sigma_L$ and σ^T were broken up into elastic and inelastic parts. From this, it can be seen that the structures in them are due principally to the inelastic contribution.

Based on existing C_{LL} data, estimates were made of the contributions to the slope of $\Delta\sigma_L$ with four-momentum transfer squared t from elastic scattering, from $pp \rightarrow \pi d$, and from $pp \rightarrow NN\pi$. The experimental results are consistent with these estimates. At the lowest energy, there is agreement with the contribution from elastic scattering alone, and at energies between 400 and 650 MeV, the results suggest that C_{LL} for $pp \rightarrow NN\pi$ should be large and negative.

The new C_{LL} data, together with other data on C_{LL} , C_{NN} , D_{NN} , D_{SS} , and D_{LS} , were used to find values of the 90° c.m. amplitudes ϕ_s , which contains only spin-singlet terms, ϕ_t , which contains only coupled-spin-triplet terms, and ϕ_T which contains only spin-triplet terms. Again, structure is apparent in the magnitudes of all of these amplitudes, which is again due to the waves 1D_2 (for ϕ_s), 3F_3 (for ϕ_T), and presumably 3P_0 or the $({}^3P_2, {}^3F_2)$ pair (for ϕ_t). The relative phases between these amplitudes ($\beta_s - \beta_t$) and ($\beta_T - \beta_t$) do not show strong energy dependence, which suggests that the structure seen in the magnitude of the amplitudes due to a single partial wave is masked by the other partial waves.

ACKNOWLEDGMENTS

We would like to thank M. McNaughton and K. McNaughton for valuable advice and help with the data acquisition, R. Damjanovich for engineering assistance, J. Boissevain for building the NMR detectors, O. Fletcher, J. Greenman, W. Haberichter, T. Kasprzyk, A. Rask, and J. Vaninetti for their assistance in setting up and running the experiment, M. J. Jacobson for the loan of the transmission counters, and the staff of the LAMPF accelerator for their assistance throughout the experiment. We would also like to thank R. A. Arndt for discussions concerning the Coulomb-nuclear corrections to the $\Delta\sigma_L$ data, and D. V. Bugg, D. A. Axen, M. Comyn, D. Healey, and R. Shypit for discussions on the comparison of the TRIUMF and LAMPF data. This work was supported in part by the U.S. Department of Energy.

APPENDIX: CORRELATED-ERROR FIT TO $\Delta\sigma_L(t_i)$

In total-cross-section experiments using transmission counters (T counters) similar to ours, the transmitted beam particles pass through many T counters. As a consequence, the errors of $\Delta\sigma(t_i)$ (obtained from the binomial distribution), where t is the four-momentum transfer squared, are correlated. The procedure used to obtain $\Delta\sigma_L$ in this situation, based on the work of Johnson,⁵⁷ is described here.

In this appendix, let $\Delta\sigma_L(t_i)$ be represented by σ_i and the corresponding error by $\delta\sigma_i$. It will be assumed that there are p counters used in the fit, with the largest T counter corresponding to σ_1 , the next largest to σ_2 , and so

on. The value of χ^2 for a fit to the σ_i is given by

$$\chi^2 = \sum_{i=1}^p \sum_{j=1}^p (\sigma_{i,\text{fit}} - \sigma_i)(V^{-1})_{ij}(\sigma_{j,\text{fit}} - \sigma_j),$$

where V is the covariance matrix of the errors

$$V_{ij} = \langle (\sigma_i - \langle \sigma_i \rangle)(\sigma_j - \langle \sigma_j \rangle) \rangle.$$

Adapting the results of Johnson⁵⁷ to our particular arrangement of the T counters, we have

$$V_{ij} = (\delta\sigma_k)^2$$

for

$$k = \min(i, j).$$

If a polynomial fit to the σ_i of degree N is assumed,

$$\sigma(t) = \sum_{m=0}^N a_m t^m,$$

then with the definitions

$$R_{ij} = (V^{-1})_{ij} = R_{ji},$$

$$H_{mn} = \sum_{i=1}^p \sum_{j=1}^p R_{ij}(t_i^m t_j^n + t_i^n t_j^m),$$

$$U_m = \sum_{i=1}^p \sum_{j=1}^p R_{ij}(\sigma_i t_j^m + \sigma_j t_i^m),$$

it can be shown that

$$a = 2(H^{-1})U$$

and that the errors on the coefficients a_m are

$$(\delta a_m)^2 = 2(H^{-1})_{mm}.$$

An explicit form for the R matrix can be found. Define

$$A_1 = 1/(\delta\sigma_1)^2$$

and

$$A_i = 1/[(\delta\sigma_i)^2 - (\delta\sigma_{i-1})^2], \quad i \geq 2.$$

It should be noted that the A_j are all positive, since

$$\delta\sigma_i < \delta\sigma_{i+1}$$

for our T counters, assuming 100% efficiency. Then,

$$R_{ij} = \begin{cases} A_i + A_{i+1}, & i = j \neq p, \\ A_i, & i = j = p, \\ -A_{i+1}, & j = i + 1, \\ 0, & |j - i| \geq 2. \end{cases}$$

The H and U matrices take the form

$$H_{mn} = 2A_1 t_1^{m+n} + 2 \sum_{i=2}^p A_i (t_i^m - t_{i-1}^m)(t_i^n - t_{i-1}^n),$$

$$U_m = 2A_1 \sigma_1 t_1^m + 2 \sum_{i=2}^p A_i (\sigma_i - \sigma_{i-1})(t_i^m - t_{i-1}^m).$$

It is apparent that the term for the largest T counter in

the fit has a special form, whereas the other σ_i and t_j appear only in differences.

In the special case of a linear fit in t ($N = 1$), the coefficients are

$$a_1 = (\text{slope}) = \frac{\sum_{i=2}^p A_i (\sigma_i - \sigma_{i-1}) (t_i - t_{i-1})}{\sum_{i=2}^p A_i (t_i - t_{i-1})^2},$$

$$a_0 = \Delta\sigma_L = \sigma_1 - a_1 t_1.$$

More complicated formulas can be written for the quadratic and higher-order fits in t .

Several general statements on these correlated error fits

can be made. As in the example of the linear fit above, the coefficients a_m for $m \geq 1$ depend only on sums over $i = 2$ to p of differences in σ_i and t_j^m , but not on A_1 . Also, it can be shown that, in general,

$$\sigma(t) = \sigma_1 + \sum_{m=1}^N a_m (t^m - t_1^m).$$

Thus, the correlated error fit anchors the fitted polynomial to $\sigma = \sigma_1$ at $t = t_1$ and uses the difference in cross section between adjacent T counters to evaluate all other coefficients a_m for $m \geq 1$. Finally, since the values of A_j ($j \geq 2$) depend on differences between squared errors on $\Delta\sigma_L(t_i)$, these errors have been quoted to several significant figures in Table IV.

*Current address: AT&T Bell Laboratories, Holmdel, New Jersey 07733.

†Current address: Department of Physics, Kyoto University, Kyoto 606, Japan.

‡Current address: IBM Japan, Ltd., Mori Bldg. 21, 4-34 Roppongi 1 Chome, Minato-Ku, Tokyo 106, Japan.

§Current address: Los Alamos National Laboratory, Los Alamos, New Mexico 87545.

**Current address: 38 Neponsit Ave., Foxboro, Massachusetts 02035.

¹I. P. Auer, E. Colton, D. Hill, K. Nield, B. Sandler, H. Spinka, Y. Watanabe, A. Yokosawa, and A. Beretvas, *Phys. Lett.* **67B**, 113 (1977); I. P. Auer, E. Colton, H. Halpern, D. Hill, H. Spinka, G. Theodosiou, D. Underwood, Y. Watanabe, and A. Yokosawa, *Phys. Rev. Lett.* **41**, 354 (1978); I. P. Auer, A. Beretvas, E. Colton, D. Hill, K. Nield, H. Spinka, D. Underwood, Y. Watanabe, and A. Yokosawa, *Phys. Lett.* **70B**, 475 (1977); H. Hidaka, A. Beretvas, K. Nield, H. Spinka, D. Underwood, Y. Watanabe, and A. Yokosawa, *ibid.* **70B**, 479 (1977).

²T. Kamae and T. Fujita, *Phys. Rev. Lett.* **38**, 471 (1977); H. Ikeda, I. Arai, H. Fujii, T. Fujii, H. Iwasaki, N. Kajiuira, T. Kamae, K. Nakamura, T. Sumiyoshi, H. Takeda, K. Ogawa, and M. Kanazawa, *ibid.* **42**, 1321 (1979); T. Ueda, *Phys. Lett.* **74B**, 123 (1978).

³R. L. Jaffe, *Phys. Rev. Lett.* **38**, 195 (1977); **38**, 617 (1977); P. J. G. Mulders, A. Th. M. Aerts, and J. J. de Swart, *ibid.* **40**, 1543 (1978); A. Th. M. Aerts, P. J. G. Mulders, and J. J. de Swart, *Phys. Rev. D* **17**, 260 (1978); P. J. Mulders, *ibid.* **25**, 1269 (1982); S. Ishida and M. Oda, *Prog. Theor. Phys.* **61**, 1401 (1979); D. B. Lichtenberg, E. Predazzi, D. H. Weingarten, and J. G. Wills, *Phys. Rev. D* **18**, 2569 (1978).

⁴B. A. Shahbazian, P. P. Temnikov, and A. A. Timonina, *Nucl. Phys.* **A374**, 73c (1982); see also H. Spinka and D. Bugg (Ref. 5).

⁵K. Hidaka and A. Yokosawa, *Surv. High Energy Phys.* **1**, 141 (1980); A. Yokosawa, *Phys. Rep.* **64**, 49 (1980); J. B. Roberts, in *Polarization Phenomena in Nuclear Physics—1980*, proceedings of the Fifth International Symposium, Sante Fe, edited by G. G. Ohlson, R. E. Brown, N. Jarmie, M. W. McNaughton, and G. M. Hale (AIP, New York, 1981), p. 31; W. M. Kloet, in *Proceedings of the Workshop on Nuclear and Particle Physics at Energies up to 31 GeV, Los Alamos, 1981*, edited by J. D. Bowman, L. S. Kisslinger, and R. R. Silbar (Los Alamos National Laboratory Report No. LANL-LA-8775-C, 1981), p. 211; H. Spinka, *ibid.*, p. 220; R. Vinh Mau,

Nucl. Phys. **A374**, 3c (1982); T. Kamae, *ibid.* **A374**, 25c (1982); D. Bugg, *ibid.* **A374**, 95c (1982); M. P. Locher, work presented at Tenth International Conference on Few Body Problems in Physics, Karlsruhe, 1983 (unpublished); P. Kroll (unpublished).

⁶I. P. Auer, E. Colton, W. R. Ditzler, D. Hill, R. Miller, H. Spinka, G. Theodosiou, J.-J. Tavernier, N. Tamura, K. Toshioka, D. Underwood, R. Wagner, A. Yokosawa, P. Kroll, and W. Jauch, *Phys. Rev. Lett.* **51**, 1411 (1983).

⁷For instance, see A. Konig and P. Kroll, *Nucl. Phys.* **A356**, 345 (1981); W. M. Kloet and R. R. Silbar, *ibid.* **A364**, 346 (1981); A. S. Rinat and R. S. Bhalerao, Weizmann Institute Report No. WIS-82/55 Nov.-Ph., 1982 (unpublished).

⁸W. deBoer, R. C. Fernow, A. D. Krisch, H. E. Miettinen, T. A. Mulera, J. B. Roberts, K. M. Terwilliger, L. G. Ratner, and J. R. O'Fallon, *Phys. Rev. Lett.* **34**, 558 (1975); see also Ref. 94.

⁹For a summary of sources of these data, see H. Spinka (Ref. 5) and D. Bugg (Ref. 5).

¹⁰N. Hoshizaki, *Prog. Theor. Phys.* **57**, 1099 (1977); **58**, 716 (1977); **60**, 1796 (1978); **61**, 129 (1979); see also B. J. Edwards and G. H. Thomas, *Phys. Rev. D* **22**, 2772 (1980); and B. J. Edwards, *ibid.* **23**, 1978 (1981).

¹¹R. Bhandari, R. A. Arndt, L. D. Roper, and B. J. VerWest, *Phys. Rev. Lett.* **46**, 1111 (1981).

¹²W. Grein and P. Kroll, *Nucl. Phys.* **B137**, 173 (1978).

¹³W. Grein and P. Kroll, *Nucl. Phys.* **A377**, 505 (1982).

¹⁴J. Bystricky, J. Deregél, F. Lehar, C. R. Newsom, J. Yonnet, J. M. Fontaine, J. Gosset, F. Perrot, C. Lechanoine-Leluc, W. R. Leo, Y. Onel, P. Winternitz, S. Colautti-Dalla Torre, A. Penzo, and H. Azaiez, Saclay Report No. DPhPE 82-09, 1982 (unpublished).

¹⁵D. V. Bugg, *J. Phys. G* **5**, 1349 (1979).

¹⁶R. Dubois, D. Axen, R. Keeler, M. Comyn, G. A. Ludgate, J. R. Richardson, N. M. Stewart, A. S. Clough, D. V. Bugg, and J. A. Edgington, *Nucl. Phys.* **A377**, 554 (1982); D. V. Bugg, J. A. Edgington, W. R. Gibson, N. Wright, N. M. Stewart, A. S. Clough, D. Axen, G. A. Ludgate, C. J. Oram, L. P. Robertson, J. R. Richardson, and C. Amsler, *Phys. Rev. C* **21**, 1004 (1980); D. V. Bugg, J. A. Edgington, C. Amsler, R. C. Brown, C. J. Oram, K. Shakarchi, N. M. Stewart, G. A. Ludgate, A. S. Clough, D. Axen, S. Jaccard, and J. Vavra, *J. Phys. G* **4**, 1025 (1978).

¹⁷C. L. Hollas, *Phys. Rev. Lett.* **44**, 1186 (1980).

¹⁸W. M. Kloet, R. R. Silbar, R. Aaron, and R. D. Amado, *Phys. Rev. Lett.* **39**, 1643 (1977); W. M. Kloet and R. R. Silbar,

- Nucl. Phys. **A338**, 281 (1980); **A338**, 317 (1980); Phys. Rev. Lett. **45**, 970 (1980); W. M. Kloet, J. A. Tjon, and R. R. Silber, Phys. Lett. **99B**, 80 (1981).
- ¹⁹J. A. Niskanen, Phys. Lett. **112B**, 17 (1982).
- ²⁰J. Bolger, E. Boschitz, G. Pröbstle, G. R. Smith, S. Mango, F. Vogler, R. R. Johnson, and J. Arvieux, Phys. Rev. Lett. **46**, 167 (1981).
- ²¹J. Arvieux, Phys. Lett. **103B**, 99 (1981).
- ²²R. J. Holt, J. R. Specht, K. Stephenson, B. Zeidman, J. S. Frank, M. J. Leitch, J. D. Moses, E. J. Stephenson, and R. M. Laszewski, Phys. Rev. Lett. **47**, 472 (1981); J. Ulbricht, V. König, W. Grüebler, P. A. Schmelzbach, B. Jenny, F. Sperisen, K. Elsener, C. Schweizer, and A. Chisholm, *ibid.* **48**, 311 (1982); W. Grüebler, J. Ulbricht, V. König, P. A. Schmelzbach, K. Elsener, C. Schweizer, M. Merdzan, and A. Chisholm, *ibid.* **49**, 444 (1982).
- ²³T. Kamae, I. Arai, T. Fujii, H. Ikeda, N. Kajjura, S. Kawabata, K. Nakamura, K. Ogawa, H. Takeda, and Y. Watase, Phys. Rev. Lett. **38**, 468 (1977); P. E. Argan, G. Audit, N. deBotton, J. L. Faure, J. Martin, C. Schuhl, G. Tamas, and E. Vincent, *ibid.* **46**, 96 (1981).
- ²⁴K. Baba, I. Endo, H. Fukuma, K. Inoue, T. Kawamoto, T. Ohsugi, Y. Sumi, T. Takeshita, S. Uehara, Y. Yano, and T. Maki, Phys. Rev. Lett. **48**, 729 (1982); see also V. G. Gorbinko, Yu. V. Zhebrovskij, L. Ya. Kolesnikov, A. L. Rubashkin, and P. V. Sorokin, Nucl. Phys. **A381**, 330 (1982).
- ²⁵J. Wainer and E. L. Lomon, Phys. Rev. D **22**, 1217 (1980); T. H. Fields and A. Yokosawa, *ibid.* **21**, 1432 (1980).
- ²⁶I. P. Auer, A. Beretvas, E. Colton, H. Halpern, D. Hill, K. Nield, B. Sandler, H. Spinka, G. Theodosiou, D. Underwood, Y. Watanabe, and A. Yokosawa, Phys. Rev. Lett. **41**, 1436 (1978).
- ²⁷I. P. Auer, W. R. Ditzler, D. Hill, K. Imai, H. Spinka, R. Stanek, K. Toshioka, D. Underwood, R. Wagner, A. Yokosawa, G. R. Burleson, W. B. Cottingham, S. J. Greene, E. W. Hoffman, S. Stuart, and J. J. Jarmer, Phys. Rev. D **24**, 2008 (1981).
- ²⁸G. R. Burleson, W. B. Cottingham, S. J. Greene, S. Stuart, E. W. Hoffman, J. J. Jarmer, I. P. Auer, W. R. Ditzler, D. Hill, K. Imai, H. Spinka, R. Stanek, K. Toshioka, D. Underwood, R. Wagner, and A. Yokosawa, Nucl. Phys. **B213**, 365 (1983).
- ²⁹E. Aprile, J. Bystricky, J. Deregel, C. Eisenegger, J. M. Fontaine, E. Heer, R. Hess, F. Lehar, W. Leo, S. Mango, Y. Onel, F. Perrot, D. Rapin, J. Vrzal, and J. Yonnet, in *High Energy Physics with Polarized Beams and Polarized Targets*, proceedings of International Symposium, Lausanne, Switzerland, 1980, edited by C. Joseph and J. Soffer (Birkhauser, Basel, 1981), p. 516; C. Lechanoine-Leluc (private communication).
- ³⁰D. Axen, R. Shypit M. Comyn, D. Healey, J. Stanley, N. M. Stewart, D. V. Bugg, J. A. Edgington, and N. Stevenson, J. Phys. G **7**, L225 (1981); see also Ref. 95.
- ³¹W. R. Ditzler, D. Hill, K. Imai, H. Shimizu, H. Spinka, R. Stanek, K. Toshioka, D. Underwood, R. Wagner, A. Yokosawa, G. R. Burleson, W. B. Cottingham, S. J. Greene, J. J. Jarmer, and R. H. Jeppesen, Phys. Rev. D **27**, 680 (1983).
- ³²R. A. Arndt (private communication).
- ³³E. P. Chamberlin, R. L. York, H. E. Williams, and E. L. Rios, in *Polarization Phenomena in Nuclear Physics—1980* (Ref. 5), p. 887.
- ³⁴See Report on the Notation Committee in *Higher Energy Polarized Beams*, proceedings of the Workshop, Ann Arbor, Michigan, 1977, edited by A. D. Krisch and A. J. Salthouse (AIP, New York, 1978).
- ³⁵E. W. Hoffman, IEEE Trans. Nucl. Sci. **NS-26**, 3995 (1979).
- ³⁶M. W. McNaughton, P. R. Bevington, H. B. Willard, E. Winkelmann, E. P. Chamberlin, F. H. Cverna, N. S. P. King, and H. Willmes, Phys. Rev. C **23**, 1128 (1981).
- ³⁷M. W. McNaughton, Los Alamos National Laboratory Report No. LA-8307-MS, 1980 (unpublished).
- ³⁸M. W. McNaughton and E. P. Chamberlin, Phys. Rev. C **24**, 1778 (1981).
- ³⁹H. Spinka, Argonne National Laboratory Report No. ANL-HEP-PR-81-34, 1981 (unpublished).
- ⁴⁰H. Spinka, E. Colton, W. R. Ditzler, H. Halpern, K. Imai, R. Stanek, N. Tamura, G. Theodosiou, K. Toshioka, D. Underwood, R. Wagner, Y. Watanabe, A. Yokosawa, G. R. Burleson, W. B. Cottingham, S. J. Greene, S. Stuart, and J. J. Jarmer, Nucl. Instrum. Methods **211**, 239 (1983).
- ⁴¹G. G. Ohlsen, Los Alamos National Laboratory Report No. LA-4451, 1970 (unpublished); G. G. Ohlsen, J. L. McKibben, G. P. Lawrence, P. W. Keaton, Jr., and D. D. Armstrong, Phys. Rev. Lett. **27**, 599 (1971).
- ⁴²M. W. McNaughton, in *Polarization Phenomena in Nuclear Physics—1980* (Ref. 5), p. 818.
- ⁴³P. R. Bevington, M. W. McNaughton, H. B. Willard, H. W. Baer, E. Winkelmann, F. Cverna, E. P. Chamberlin, N. S. P. King, R. R. Stevens, H. Willmes, and M. A. Schardt, Phys. Rev. Lett. **41**, 384 (1978).
- ⁴⁴L. Wolfenstein, Phys. Rev. **75**, 1664 (1949).
- ⁴⁵For recent reviews of dynamic nuclear polarization, see A. Abragam and M. Goldman, Rep. Prog. Phys. **41**, 395 (1978); V. A. Atsarkin, Usp. Fiz. Nauk. **126**, 3 (1978) [Sov. Phys. Usp. **21**, 725 (1978)].
- ⁴⁶A. deLesquen, B. Amblard, R. Beurtey, G. Cozzika, J. Bystricky, J. Deregel, Y. Ducros, J. M. Fontaine, A. Gaidot, M. Hansroul, F. Lehar, J. P. Merlo, S. Miyashita, J. Movchet, and L. van Rossum, Phys. Lett. **40B**, 277 (1972); J. Deregel, J. Bystricky, G. Cozzika, Y. Ducros, A. Gaidot, F. Lehar, A. deLesquen, J. P. Merlo, S. Miyashita, J. Movchet, L. van Rossum, B. Amblard, J. M. Fontaine, and M. Hansroul, *ibid.* **43B**, 338 (1973).
- ⁴⁷H. Desportes, in *Proceedings of the Second International Conference on Magnet Technology*, edited by I. I. Richmond and D. W. Parker (Oxford University Press, London, 1967), p. 603.
- ⁴⁸P. Autones, J. C. Brisson, A. Boucherie, G. Cozzika, J. Deregel, J. P. Duthil, H. Desportes, Y. Ducros, A. Katz, A. deLesquen, J. P. Merlo, J. F. Mougel, J. Movchet, J. C. Raoul, B. Tsai, L. van Rossum, B. Amblard, J. M. Fontaine, M. Hansroul, and J. M. Rieubland, Nucl. Instrum. Methods **103**, 211 (1972).
- ⁴⁹J. C. Raoul, P. Autones, R. Auzolle, C. Bruneton, J. Bystricky, G. Cozzika, J. Deregel, Y. Ducros, A. Gaidot, A. Katz, F. Khantine-Langlois, F. Lehar, A. deLesquen, J. P. Merlo, S. Miyashita, J. Movchet, J. Pierrard, M. Ramadier, P. Roubeau, G. Souchere, L. van Rossum, A. A. Derevschikov, N. I. Golovnya, Yu. S. Khoderev, Yu. A. Matulenko, A. P. Meschanin, S. B. Nurushev, A. I. Saraykin, V. S. Seleznev, V. V. Siskin, E. V. Smirnov, V. L. Solovyanov, V. N. Zapolsky, Yu. M. Kazarinov, M. Yu. Kazarinov, B. A. Khatchaturov, I. K. Potashnikova, and V. P. Kanavets, Nucl. Instrum. Methods, **125**, 585 (1975).
- ⁵⁰P. Roubeau, in *Proceedings of the Second International Conference on Polarized Targets*, edited by G. Shapiro (University of California Report No. LBL-500, 1971), p. 47.
- ⁵¹G. Court, in *Proceedings of the Second Workshop on Polarized Target Materials*, edited by G. R. Court, S. F. J. Cox, D. A. Cragg, and T. O. Niinikoski (Rutherford and Appleton La-

- boratories Report No. RL-80-080, 1980), p. 76.
- ⁵²I. P. Auer, D. Bridges, T. Droege, D. Hill, R. Giese, R. Miller, K. Nield, P. Rynes, B. Sandler, A. Yokosawa, G. Hicks, D. Miller, and C. Wilson, *Phys. Rev. D* **24**, 1771 (1981).
- ⁵³D. Miller, C. Wilson, R. Giese, D. Hill, K. Nield, P. Rynes, B. Sandler, and A. Yokosawa, *Phys. Rev. D* **16**, 2016 (1977).
- ⁵⁴K. Nield and R. Daly, Argonne National Laboratory Report No. ANL-HEP-PR-77-32, 1977 (unpublished).
- ⁵⁵The design was similar to that of G. Badhwar (private communication).
- ⁵⁶M. J. Jakobson, G. R. Bureson, J. R. Calarco, M. D. Cooper, D. C. Hagerman, I. Halpern, R. H. Jeppesen, K. F. Johnson, L. D. Knutson, R. E. Marrs, H. O. Meyer, and R. P. Redwine, *Phys. Rev. Lett.* **38**, 1201 (1977).
- ⁵⁷K. F. Johnson, Ph. D. thesis, New Mexico State University, 1976, Los Alamos National Laboratory Report No. LA-6561-T.
- ⁵⁸R. H. Jeppesen, Ph. D. thesis, New Mexico State University, 1980, Los Alamos National Laboratory Report No. LA-8190-T.
- ⁵⁹D. V. Bugg, A. J. Oxley, J. A. Zoll, J. G. Rushbrooke, V. E. Barnes, J. B. Kinson, W. P. Dodd, G. A. Doran, and L. Riddiford, *Phys. Rev.* **133**, B1017 (1964).
- ⁶⁰P. R. Bevington, in *Nucleon-Nucleon Interactions—1977*, proceedings of the Second International Conference, Vancouver, edited by H. Fearing, D. Measday, and A. Strathdee, (AIP, New York, 1978), p. 305; F. H. Cverna, P. R. Bevington, M. W. McNaughton, H. B. Willard, N. S. P. King, and D. R. Giebink, *Phys. Rev. C* **23**, 1698 (1981).
- ⁶¹Ch. Weddigen, *Nucl. Phys.* **A312**, 330 (1978), and references contained therein.
- ⁶²I. P. Auer, W. R. Ditzler, D. Hill, H. Spinka, N. Tamura, G. Theodosiou, K. Toshioka, D. Underwood, R. Wagner, and A. Yokosawa, *Phys. Rev. Lett.* **46**, 1177 (1981).
- ⁶³O. K. Rice, *J. Chem. Phys.* **12**, 1 (1944).
- ⁶⁴G. D. Scott and D. M. Kilgour, *Br. J. Appl. Phys.* **2**, 863 (1969).
- ⁶⁵K. Gotoh, W. S. Jodrey, and E. M. Tory, *Powder Technol.* **20**, 257 (1978).
- ⁶⁶G. D. Scott, *Nature (London)* **188**, 908 (1960).
- ⁶⁷S. Stuart, M. S. thesis, New Mexico State University, 1982, Los Alamos National Laboratory Report No. LA-9405-T.
- ⁶⁸R. A. Fisher, *Statistical Methods for Research Workers* (Oliver and Boyd, Edinburgh and London, 1958).
- ⁶⁹L. Ratner, C. Potts, and E. Parker (private communication).
- ⁷⁰D. Axen, D. V. Bugg, M. Comyn, and R. Shypit (private communication).
- ⁷¹R. A. Arndt, L. D. Roper, R. A. Bryan, R. B. Clark, B. J. VerWest, and P. Signell, *Phys. Rev. D* **28**, 97 (1983); R. A. Arndt and L. D. Roper, VPI *N-N* interactive dial-in-computing facility (manual available from Department of Physics, VPI, Blacksburg, VA 24061). (This interactive computer program is also available on computers at Argonne, LAMPF, and TRIUMF.) The phase-shift set generally used was SP82.
- ⁷²Y. Watanabe, *Phys. Rev. D* **19**, 1022 (1979).
- ⁷³J. L. Beveridge, M. K. Craddock, G. Dutto, G. H. Mackenzie, C. Oram, L. W. Root, G. Roy, and P. W. Schmor, *IEEE Trans. Nucl. Sci.* **26**, 3215 (1979).
- ⁷⁴M. Jacob and G. C. Wick, *Ann. Phys. (N.Y.)* **7**, 404 (1959).
- ⁷⁵M. L. Goldberger, M. T. Grisaru, S. W. MacDowell, and D. Y. Wong, *Phys. Rev.* **120**, 2250 (1960).
- ⁷⁶F. Halzen and G. H. Thomas, *Phys. Rev. D* **10**, 344 (1974).
- ⁷⁷A. Scotti and D. Y. Wong, *Phys. Rev.* **138**, B145 (1965).
- ⁷⁸M. E. Rose, *Elementary Theory of Angular Momentum* (Wiley, New York, 1957).
- ⁷⁹H. Spinka, Argonne Report No. ANL-HEP-CP-80-78, 1980 (unpublished); see also H. Spinka (Ref. 5).
- ⁸⁰O. Chamberlain, E. Segrè, and C. Wiegand, *Phys. Rev.* **83**, 923 (1951), as quoted in Ref. 83.
- ⁸¹J. Marshall, L. Marshall, and A. V. Nedzel, *Phys. Rev.* **91**, 767 (1953).
- ⁸²O. Chamberlain, G. Pettengill, E. Segrè, and C. Wiegand, *Phys. Rev.* **93**, 1424 (1954), as quoted in Ref. 83.
- ⁸³H. G. Carvalho, *Phys. Rev.* **96**, 398 (1954).
- ⁸⁴V. P. Dzhelepov, V. I. Moskalev, and S. V. Medved, *Doklady Akad. Nauk. SSSR* **104**, 380 (1955).
- ⁸⁵M. G. Meshcheryakov, N. P. Bogachev, and B. S. Neganov, *Nuovo Cimento Suppl.* **3**, 119 (1956).
- ⁸⁶F. F. Chen, C. P. Leavitt, and A. M. Shapiro, *Phys. Rev.* **103**, 211 (1956).
- ⁸⁷M. E. Law, G. W. Hutchinson, and D. H. White, *Nucl. Phys.* **2**, 600 (1959).
- ⁸⁸M. J. Longo, J. A. Helland, W. N. Hess, B. J. Moyer, and V. Perez-Mendez, *Phys. Rev. Lett.* **3**, 568 (1959).
- ⁸⁹M. J. Longo and B. J. Moyer, *Phys. Rev.* **125**, 701 (1962).
- ⁹⁰V. M. Guzhavin, G. K. Kliger, V. Z. Kolganov, A. V. Lebedev, K. S. Marish, Yu. D. Prokoshkin, V. T. Smolyanin, A. P. Sokolov, L. M. Soroko, and Ts'ui Wa-Ch'uang *Zh. Eksp. Teor. Fiz.* **46**, 1245 (1964) [*Sov. Phys. JETP* **19**, 847 (1964)].
- ⁹¹D. V. Bugg, D. C. Salter, G. H. Stafford, R. F. George, K. F. Riley, and R. J. Tapper, *Phys. Rev.* **146**, 980 (1966).
- ⁹²G. J. Igo, J. L. Friedes, H. Palevsky, R. Sutter, G. Bennett, W. D. Simpson, D. M. Corley, and R. L. Stearns, *Nucl. Phys.* **B3**, 181 (1967).
- ⁹³P. Schwaller, M. Pepin, B. Favier, C. Richard-Serre, D. F. Measday, and P. U. Renberg, *Nucl. Phys.* **A316**, 317 (1979).
- ⁹⁴Ed. K. Biegert, J. A. Buchanan, J. M. Clement, W. H. Dragoset, R. D. Felder, J. H. Hoftiezer, K. R. Hogstrom, J. Hudomalj-Gabitzsch, J. D. Lesikar, W. P. Madigan, G. S. Mutchler, G. C. Phillips, J. B. Roberts, T. M. Williams, K. Abe, R. C. Fernow, T. A. Mulera, S. Bart, B. W. Mayes, and L. Pinsky, *Phys. Lett.* **73B**, 235 (1978).
- ⁹⁵J. P. Stanley, N. M. Stewart, D. V. Bugg, J. A. Edgington, N. R. Stevenson, A. S. Clough, D. A. Axen, R. Shypit, M. Comyn, D. Healey, and G. A. Ludgate, *Nucl. Phys.* **A403**, 525 (1983).
- ⁹⁶J. Bystricky, J. Deregél, J. M. Fontaine, J. Gosset, F. Lehar, C. R. Newsom, F. Perrot, C. A. Whitten, and J. Yonnet, work presented at the Ninth International Conference on High Energy Physics and Nuclear Structure, Versailles, 1981 (unpublished).
- ⁹⁷See R. Dubois *et al.* (Ref. 16).
- ⁹⁸I. P. Auer, E. Colton, W. R. Ditzler, D. Hill, R. Miller, H. Spinka, G. Theodosiou, J. J. Tavernier, N. Tamura, K. Toshioka, D. Underwood, R. Wagner, A. Yokosawa, P. Kroll, and W. Jauch, *Phys. Rev. Lett.* **51**, 1411 (1983).
- ⁹⁹R. Hess, in *High Energy Physics with Polarized Beams and Polarized Targets* (Ref. 29).
- ¹⁰⁰J. Marshall, L. Marshall, and V. A. Nedzel, *Phys. Rev.* **92**, 834 (1953), as quoted in Ref. 83.
- ¹⁰¹R. B. Sutton, T. H. Fields, J. G. Fox, J. A. Kane, W. E. Mott, and R. A. Stallwood, *Phys. Rev.* **97**, 783 (1955).
- ¹⁰²L. W. Smith, A. W. McReynolds, and G. Snow, *Phys. Rev.* **97**, 1186 (1955).
- ¹⁰³J. Marshall, L. Marshall, and V. A. Nedzel, *Phys. Rev.* **98**, 1513 (1955).

- ¹⁰⁴T. W. Morris, E. C. Fowler, and J. D. Garrison, *Phys. Rev.* **103**, 1472 (1956).
- ¹⁰⁵N. P. Bogachev, *Sov. Phys. Doklady* **1**, 361 (1956).
- ¹⁰⁶T. Elioff, L. Agnew, O. Chamberlain, H. Steiner, C. Wiegand, and T. Ypsilantis, *Phys. Rev. Lett.* **3**, 285 (1959).
- ¹⁰⁷W. K. McFarlane, R. J. Homer, A. W. O'Dell, E. J. Sacharidis, and G. H. Eaton, *Nuovo Cimento* **28**, 943 (1963).
- ¹⁰⁸T. A. Murray, L. Riddiford, G. H. Grayer, T. W. Jones, and Y. Tanimura, *Nuovo Cimento* **49A**, 261 (1967).
- ¹⁰⁹M. Arik and P. G. Williams, *Nucl. Phys.* **B136**, 425 (1978).
- ¹¹⁰J. Bystricky and F. Lehar, in *Proceedings of the Fourth International Symposium on Polarization Phenomena in Nuclear Reactions*, edited by W. Gruebler and V. Konig (Birkhauser, Zurich, 1976), p. 458.
- ¹¹¹J. Bystricky, F. Lehar, and P. Winternitz, *J. Phys. (Paris)* **39**, 1 (1978).
- ¹¹²D. V. Bugg, J. A. Edgington, W. R. Gibson, N. Wright, N. M. Stewart, A. S. Clough, D. Axen, G. A. Ludgate, C. J. Oram, L. P. Robertson, J. R. Richardson, and C. Amsler, *Phys. Rev. C* **21**, 1004 (1980).
- ¹¹³E. Aprile, R. Hausammann, E. Heer, R. Hess, C. Lechanoine-Leluc, W. R. Leo, S. Morenzoni, Y. Onel, D. Rapin, and S. Mango, work presented at Conference on Polarization Phenomena in Nuclear Physics, Sante Fe, 1980 (unpublished); C. Lechanoine-Leluc (private communication).
- ¹¹⁴T. S. Bhatia, J. G. J. Boissevain, J. J. Jarmer, R. R. Silbar, J. E. Simmons, G. Glass, J. C. Hiebert, R. A. Kenefick, L. C. Northcliffe, W. B. Tippens, W. M. Kloet, and J. Dubach, *Phys. Rev. C* **28**, 2071 (1983).
- ¹¹⁵R. Shypit, C. E. Waltham, D. A. Axen, F. Entezami, M. Comyn, D. Healey, G. A. Ludgate, G. D. Wait, D. V. Bugg, J. A. Edgington, and N. R. Stevenson, *Phys. Lett.* **124B**, 314 (1983).
- ¹¹⁶M. H. MacGregor, M. J. Moravcsik, and H. P. Stapp, *Annu. Rev. Nucl. Sci.* **10**, 291 (1960).
- ¹¹⁷Yu. P. Kumeikin, M. G. Meshcheryakov, S. B. Nurushv, and G. D. Stoletov, *Zh. Eksp. Teor. Fiz.* **43**, 1665 (1962) [*Sov. Phys. JETP* **16**, 1175 (1963)]; **46**, 50 (1964) [**19**, 36 (1964)].
- ¹¹⁸A. W. Hendry, *Phys. Rev. D* **23**, 2075 (1981).
- ¹¹⁹A. Svarc, Z. Bajzer, and M. Furic, *Nucl. Phys.* **A370**, 468 (1981).
- ¹²⁰G. R. Goldstein and M. J. Moravcsik, *Phys. Rev. D* **26**, 3026 (1982).
- ¹²¹O. Chamberlain, E. Segrè, and C. Wiegand, *Phys. Rev.* **83**, 923 (1951).
- ¹²²N. P. Bogachev and I. K. Vzorov, *Dok. Akad. Nauk SSSR* **99**, 931 (1954). A translation of the information in this reference and in Refs. 123 and 124 is given in M. G. Meshcheryakov, N. P. Bogachev, and B. S. Neganov, *Nuovo Cimento Suppl.* **3**, 119 (1956).
- ¹²³M. G. Meshcheryakov, N. P. Bogachev, B. S. Neganov, and E. V. Piskarev, *Dok. Akad. Nauk. SSSR* **99**, 955 (1954).
- ¹²⁴M. G. Meshcheryakov, B. S. Neganov, L. M. Soroko, and I. K. Vzorov, *Dok. Akad. Nauk. SSSR* **99**, 959 (1954).
- ¹²⁵S. J. Nikitin, J. M. Selector, E. G. Bogomolov, and S. M. Zombkovskij, *Nuovo Cimento* **2**, 1269 (1955).
- ¹²⁶O. Chamberlain, E. Segre, R. D. Tripp, C. Wiegand, and T. Ypsilantis, *Phys. Rev.* **105**, 288 (1957).
- ¹²⁷D. Harting, J. R. Holt, and J. A. Moore, *Proc. Phys. Soc. London* **71**, 770 (1958).
- ¹²⁸V. M. Guzhavein, G. K. Kliger, V. Z. Kolganov, A. V. Lebedev, K. S. Marish, M. A. Musin, Yu. D. Prokoshkin, V. T. Smolyankin, A. P. Sokolov, L. M. Soroko, and Ts'ui Wa-Ch'uang, *Zh. Eksp. Teor. Fiz.* **47**, 1228 (1964) [*Sov. Phys. JETP* **20**, 830 (1965)].
- ¹²⁹B. B. Brabson, R. R. Crittenden, R. M. Heinz, R. C. Kammerud, H. A. Neal, H. W. Paik, R. A. Sidwell, and K. F. Suen, *Phys. Rev. Lett.* **23**, 1306 (1969); R. C. Kammerud, B. B. Brabson, R. R. Crittenden, R. M. Heinz, H. A. Neal, H. W. Paik, and R. A. Sidwell, *Phys. Rev. D* **4**, 1309 (1971).
- ¹³⁰M. G. Albrow, S. Andersson/Almehed, B. Bosnjakovic, C. Daum, F. C. Erne, J. P. Lagnaux, J. C. Sens, and F. Udo, *Nucl. Phys.* **B23**, 445 (1970).
- ¹³¹B. A. Ryan, A. Kanofsky, T. J. Devlin, R. E. Mischke, and P. F. Shepard, *Phys. Rev. D* **3**, 1 (1971).
- ¹³²D. T. Williams, I. J. Bloodworth, E. Eisenhandler, W. R. Gibson, P. I. P. Kalmus, L. C. Y. Lee Chi Kwong, G. T. J. Arnison, A. Astbury, S. Gjesdal, E. Lillethun, B. Stave, O. Ullaland, and I. L. Watkins, *Nuovo Cimento* **8A**, 447 (1972).
- ¹³³K. Abe, B. A. Barnett, J. H. Goldman, A. T. Laasanen, P. H. Steinberg, G. J. Marmer, D. R. Moffett, and E. F. Parker, *Phys. Rev. D* **12**, 1 (1975).
- ¹³⁴H. B. Willard, B. D. Anderson, H. W. Baer, R. J. Barrett, P. R. Bevington, A. N. Anderson, H. Willmes, and N. Jarmie, *Phys. Rev. C* **14**, 1545 (1976).
- ¹³⁵P. Chatelain, B. Favier, F. Foroughi, J. Hoftiez, S. Jaccard, J. Piffaretti, P. Walden, and C. Weddigen, *J. Phys. G* **8**, 643 (1982).
- ¹³⁶M. L. Barlett, G. W. Hoffmann, J. A. McGill, B. Hoistad, L. Ray, R. W. Ferguson, E. C. Milner, J. A. Marshall, J. F. Amann, B. E. Bonner, J. B. McClelland, G. S. Blanpied, and R. A. Arndt, *Phys. Rev. C* **27**, 682 (1983).
- ¹³⁷J. V. Allaby, A. Ashmore, A. N. Diddens, J. Eades, G. B. Huxtable, and K. Skarsvag, *Proc. Phys. Soc. London* **77**, 234 (1961).
- ¹³⁸B. M. Golovin, V. P. Dzhelepov, and R. Ya. Zul'karneev, *Zh. Eksp. Teor. Fiz.* **41**, 83 (1961) [*Sov. Phys. JETP* **14**, 63 (1962)].
- ¹³⁹E. Engels, T. Bowen, J. W. Cronin, R. L. McIlwain, and L. G. Pondrom, *Phys. Rev.* **129**, 1858 (1963).
- ¹⁴⁰I. M. Vasilevskii, V. V. Vishnyakov, E. Iliesku, and A. A. Tyapkin, *Zh. Eksp. Teor. Fiz.* **45**, 474 (1963) [*Sov. Phys. JETP* **18**, 327 (1964)].
- ¹⁴¹G. Coignet, D. Cronenberger, K. Kuroda, A. Michalowicz, J. C. Oliver, M. Poulet, J. Teillac, M. Borghini, and C. Ryter, *Nuovo Cimento* **43A**, 708 (1966).
- ¹⁴²H. E. Dost, J. F. Arens, F. W. Betz, O. Chamberlain, M. J. Hansroul, L. E. Holloway, C. H. Schultz, and G. Shapiro, *Phys. Rev.* **153**, 1394 (1967).
- ¹⁴³G. Cozzika, Y. Ducros, A. deLesquen, J. Movchet, J. C. Raoul, L. van Rossum, J. Deregél, and J. M. Fontaine, *Phys. Rev.* **164**, 1672 (1967).
- ¹⁴⁴B. M. Golovin, R. Ya. Zul'karneev, V. S. Kiselev, S. V. Medved, V. I. Nikanorov, A. F. Pisarev, and G. L. Semashko, *Yad. Fiz.* **5**, 146 (1967) [*Sov. J. Nucl. Phys.* **5**, 101 (1967)].
- ¹⁴⁵A. Beretvas, *Phys. Rev.* **171**, 1392 (1968).
- ¹⁴⁶O. N. Jarvis, T. W. P. Brogden, B. Rose, J. P. Scanlon, J. Orchard-Webb, and M. R. Wigan, *Nucl. Phys.* **A108**, 63 (1968).
- ¹⁴⁷A. Lin, J. R. O'Fallon, L. G. Ratner, P. F. Schultz, K. Abe, D. G. Crabb, R. C. Fernow, A. D. Krisch, A. J. Salthouse, B. Sandler, and K. M. Terwilliger, *Phys. Lett.* **74B**, 273 (1978).
- ¹⁴⁸D. Besset, Q. H. Do, B. Favier, R. Hausammann, E. Heer, R. Hess, C. Lechanoine-Leluc, W. R. Leo, D. Rapin, D. W. Werren, Ch. Weddigen, J. M. Cameron, S. Jaccard, and S. Mango, *Nucl. Phys.* **A345**, 435 (1980).
- ¹⁴⁹D. A. Bell, J. A. Buchanan, M. M. Calkin, J. M. Clement, W. H. Dragoset, M. Furic, K. A. Johns, J. D. Lesikar, H. E.

- Miettinen, T. A. Mulera, G. S. Mutchler, G. C. Phillips, J. B. Roberts, and S. E. Turpin, *Phys. Lett.* **94B**, 310 (1980).
- ¹⁵⁰M. W. McNaughton, H. W. Baer, P. R. Bevington, F. H. Cverna, H. B. Willard, E. Winkelmann, E. P. Chamberlin, J. J. Jarmer, N. S. P. King, J. E. Simmons, M. A. Schardt, and H. Willmes, *Phys. Rev. C* **23**, 838 (1981).
- ¹⁵¹V. A. Efimov, A. I. Kovalev, V. V. Poljakov, V. E. Popov, A. N. Prokofiev, A. V. Shvedchikov, V. Yu. Trautman, V. G. Vovchenko, A. A. Zhdanov, N. S. Borisov, M. Yu. Kazarinov, Yu. M. Kazarinov, Yu. F. Kiselev, M. Yu. Liburg, B. S. Neganov, and Yu. A. Usov, *Phys. Lett.* **99B**, 28 (1981).
- ¹⁵²M. W. McNaughton, E. P. Chamberlin, J. J. Jarmer, N. S. P. King, H. B. Willard, and E. Winkelmann, *Phys. Rev. C* **25**, 2107 (1982).
- ¹⁵³T. S. Bhatia, G. Glass, J. C. Hiebert, R. A. Kenefick, L. C. Northcliffe, W. B. Tippens, J. G. J. Boissevain, J. J. Jarmer, J. E. Simmons, G. E. Tripard, D. Fitzgerald, J. Holt, and A. Mokhtari, *Phys. Rev. Lett.* **49**, 1135 (1982).
- ¹⁵⁴V. I. Nikanorov, G. Peter, A. F. Pisarev, and Kh. Pose, *Zh. Eksp. Teor. Fiz.* **42**, 1209 (1962) [*Sov. Phys. JETP* **15**, 837 (1962)].
- ¹⁵⁵E. Aprile, R. Hausammann, E. Heer, R. Hess, C. Lechanoine-Leluc, W. Leo, S. Morenzoni, Y. Onel, D. Rapin, and S. Mango, *Phys. Rev. D* **28**, 21 (1983).
- ¹⁵⁶P. Catillon, M. Chapellier, and D. Garreta, *Nucl. Phys.* **B2**, 93 (1967).
- ¹⁵⁷M. I. Dzhgarkava, Yu. M. Kazarinov, I. Strakhota, and M. R. Khayatov, *Yad. Fiz.* **35**, 65 (1982); [*Sov. J. Nucl. Phys.* **35**, 39 (1982)].
- ¹⁵⁸J. A. Kane, R. A. Stallwood, R. B. Sutton, and J. G. Fox, *Bull. Am. Phys. Soc.* **1**, 9 (1956).
- ¹⁵⁹Yu. P. Kumeikin, M. G. Meshcheryakov, S. B. Nurusev, and G. D. Stoletov, *Zh. Eksp. Teor. Fiz.* **38**, 1451 (1960) [*Sov. Phys. JETP* **11**, 1049 (1960)].
- ¹⁶⁰R. Roth, E. Engels, S. C. Wright, P. Kloeppe, R. Handler, and L. G. Pondrom, *Phys. Rev.* **140**, B1533 (1965).
- ¹⁶¹S. C. Wright, D. Shawhan, L. Pondrom, S. Olsen, and R. Handler, *Phys. Rev.* **175**, 1704 (1968).
- ¹⁶²J. Bystricky, J. Cech, Z. Janout, Yu. M. Kazarinov, F. Lehar, and L. B. Parfenov, *Phys. Lett.* **28B**, 572 (1969).
- ¹⁶³R. Ya. Zul'karneev, V. S. Nadezhdin, and V. I. Satarov, *Yad. Fiz.* **11**, 178 (1970) [*Sov. J. Nucl. Phys.* **11**, 98 (1970)].
- ¹⁶⁴V. G. Vovchenko, A. A. Zhdanov, V. M. Zheleznyakov, Yu. M. Kazarinov, E. N. Komarov, V. V. Polyakov, O. Ya. Fedorov, A. V. Shvedchikov, and S. V. Yazikova, *Yad. Fiz.* **25**, 975 (1977) [*Sov. J. Nucl. Phys.* **25**, 519 (1977)].
- ¹⁶⁵E. Aprile, C. Eisenegger, R. Hausammann, E. Heer, R. Hess, C. Lechanoine-Leluc, W. R. Leo, S. Morenzoni, Y. Onel, D. Rapin, and S. Mango, *Phys. Rev. Lett.* **46**, 1047 (1981).
- ¹⁶⁶M. W. McNaughton, B. E. Bonner, W. D. Cornelius, E. W. Hoffman, O. B. van Dyck, R. L. York, R. D. Ransome, C. L. Hollas, P. J. Riley, and K. Toshioka, *Phys. Rev. C* **25**, 1967 (1982).
- ¹⁶⁷B. E. Bonner and M. W. McNaughton (private communication).
- ¹⁶⁸B. M. Golovin, R. Ya. Zul'karneev, V. S. Kiselev, S. V. Medved, V. I. Nikanorov, A. F. Pisarev, and G. L. Semashko, *Yad. Fiz.* **6**, 804 (1967) [*Sov. J. Nucl. Phys.* **6**, 585 (1968)].
- ¹⁶⁹M. W. McNaughton, B. E. Bonner, E. W. Hoffman, O. B. van Dyck, C. L. Hollas, P. J. Riley, K. H. McNaughton, K. Imai, K. Toshioka, J. Roberts, S. E. Turpin, B. Aas, and A. Rahbar, *Phys. Rev. C* **26**, 249 (1982).